UiT The Arctic University of Norway

The Faculty of Health Sciences

An Investigation into the Effects of Chronic High Fructose Consumption on Liver Histology, Triglyceride Content and Gene Expression in Male Sprague-Dawley Rats

John Martin Ming Fredriksen

Master's thesis in Clinical Nutrition, ERN-3900, May 2024

Main supervisor: Neoma Boardman, Associate Professor, Department of Medical Biology

Co-supervisor: Astri Jeanette Meen, Associate Professor, Department of Medical Biology

Acknowledgements

This master's thesis was written at the Department of Medical Biology, UiT The Arctic University of Norway. It was written under the guidance of main supervisor, associate professor Neoma Tove Boardman, and co-supervisor, associate professor Astri Jeanette Meen. All experimental work was conducted at the facilites of the Cardiovascular Research Group and the Advanced Microscopy Core Facility.

I would like to thank my main supervisor, Neoma Tove Boardman, for her advice, patience, and enthusiasm. I was struggling with fatigue and a severe lack of motivation at the end of last summer, but Neoma has been incredibly patient and understanding, and has helped make this an enjoyable and valuable experience. I also want to thank Astri for her valuable feedback on my thesis structure and writing.

Furthermore, I want to thank lab engineer Aud-Malin Karlsson Hovd, Palara Anthimi, and Trine Lund, for helping me to conduct my experimental work. I would also like to thank PhD candidate in statistics/epidemiology, Andrew Mashchak, for helping me with R programming and statistics.

A huge thanks also goes out to my best friend and classmate, Thomas Torjussen, for somehow managing to convince me to not take a gap year last summer. I don't regret it now.

I am also extremely thankful to my parents and sister for always supporting me.

Finally, to all my friends, fellow students, and lecturers: When I arrived with Hurtigruten in Tromsø five years ago, I looked across the city and wondered what life would be like during and after these five years. I was not disappointed. Thank you for making this period one of the best times of my life.

Tromsø, May 2024
John Martin Ming Fredriksen

Lists of Abbreviations

AMCF = Advanced Microscopy Core Facility

ATF4 = Activating transcription factor 4

bHLH-LZ = Basic-helix-loop-leucine zipper

cDNA = Complementary DNA

CHOP = C/EBP homologous protein

ChREBP = Carbohydrate-responsive element-binding protein

CM = Chylomicrons

COL1A1 = Collagen, type I, alpha 1

COL3A1 = Collagen, type III, alpha 1

CPT1 = Carnitine palmitoyl transferase-1

Cq = cycle of quantification

Ct = Cycle threshold

DHAP = Dihydroxy acetone phosphate

DNL = De novo lipogenesis

FFA = Free fatty acids

FGF21 = Fibroblast growth factor-21

FGFR1c = Fibroblast growth factor receptor 1c

GA = Glyceraldehyde

GA3P = Glyceraldehyde-3-phosphate

H&E = Hematoxylin and eosin

HFCS = High-fructose corn syrup

HSCs = Hepatic stellate cells

HVPG = Hepatic venous pressure gradient

IL-6 = Interleukin 6

IMB = Department of Medical Biology

Klb = b-klotho

MAFLD = Metabolic-dysfunction associated fatty liver disease

MetS = Metabolic syndrome

mRNA = Messenger RNA

NAFLD = Non-alcoholic fatty liver disease

NASH = Non-alcoholic steatohepatitis

OCT = Optimal cutting temperature

ORO = Oil Red O

PDC = Pyruvate dehydrogenase complex

PDK4 = Pyruvate dehydrogenase kinase 4

PFK-1 = Phosphofructokinase-1

PH = Portal hypertension

PPARa = Peroxisome proliferator-activated receptor alpha

PPARa = Peroxisome proliferator-activated receptor gamma

PPARGC1A = Peroxisome proliferator-activated receptor gamma coactivator 1-alpha

PPARs = Peroxisome proliferator-activated receptors

PSR = Picro sirius red

SREBP = Sterol regulatory element binding protein

TNF-a = Tumor necrosis factor alpha

tRNA = Transfer RNA

UPR = Ufolded protein response

VLDL = Very low density lipoproteins

Table of Contents

List of tables

List of figures

Abstract

Bakgrunn: Kronisk høyt fruktoseintak er assosiert med metabolsk syndrom (MetS) og metabolsk dysfunksjonsassosiert fettlever (MAFLD). Fruktosemetabolisme i leveren er ikke regulert på samme måte som glukosemetabolisme, og høyt fruktoseinntak kan derfor øke fettsyntese og fettlagring i leveren som over tid fører til ugunstige metabolske endringer. Fruktose kan også føre til hypertensjon og remodellering av hjertevev, men mekanismene er ikke helt forstått. Fibroblast growth factor 21 (FGF21) er økt ved metabolsk stress og kan spille en rolle i å beskytte mot fruktose-induserte skader.

Formål: I denne masteroppgaven var formålet å undersøke effekten av kronisk høyt fruktoseinntak på leverens histologi, triglyseridenivåer og genuttrykk i et eksperimentelt rotteforsøk.

Metode: 24 hankjønnede Sprague-Dawley rotter er tidligere blitt randomisert til en fruktosegruppe og en kontrollgruppe i 16 uker. Begge gruppene fikk ad-libitum tilgang på standard tørrfôr, og 15% fruktose ble tilsatt drikkevannet til fruktosegruppen. Rottene ble avlivet etter 16 uker og leveren deres ble lagret i omtrent 1 år før oppstart av denne masteroppgaven. I denne oppgaven ble rottelevrene undersøkt ved hjelp av hematoksylin og eosin (H&E) farging, Picro Sirius Red (PSR) farging, og Oil Red O (ORO) farging. Deretter ble et triglyseridassay brukt for å kvantifisere triglyseridinnholdet i levrene, og reverse transcription quantitative polymerase chain reaction (RT-qPCR) ble utført for å undersøke om det var forskjeller i uttrykk av gener knyttet til krysskommunikasjon mellom ulike organer, fettsyremetabolisme, cellulært stress, inflammasjon, og fibrose.

Resultater: Mengden makrovesikulær og mikrovesikulær hepatisk steatose, lipiddråper, og triglyserider var signifikant høyere i fruktosegruppen sammenlignet mot kontrollgruppen, men uten forskjell i kollageninnhold. mRNA nivåer av *Atf4* og *Fgf21*, relatert til cellulært stress og trolig inter-organ krysskommunikasjon, var oppregulert i fruktosegruppen, mens *Pdk4* som er viktig for regulering av glukose og fettmetabolisme var nedregulert.

Konklusjon: Resultatene fra denne masteroppgaven viser at kronisk inntak av en 15% fruktosedrikke påvirker levermetabolismen og fører til økt grad av leversteatose men fører ikke til økt kollageninnhold.

Abstract

Background: Chronic high fructose intake is associated with the metabolic syndrome (MetS) and metabolic-dysfunction associated fatty liver disease (MAFLD). Fructose metabolised in the liver is not subject to the same strict regulation as glucose, and high fructose intake can therefore increase lipid production and storage, leading to detrimental metabolic changes. Fructose may also induce hypertension and cardiac remodeling, with mechanisms yet to be fully understood. Fibroblast growth factor 21 (*Fgf21*), elevated during metabolic stress, may play a role in mitigating fructose-induced damage.

Aims: The aim of this master's project was to investigate the effects of a high fructose intervention on liver histology, liver triglyceride content, and liver gene expression in an experimental rat model of MAFLD.

Methods: 24 male Sprague-Dawley rats were previously randomised into a fructose group and a control group for 16 weeks. Both groups were given an ad-libitum standard chow diet, and 15% fructose was administered to the drinking water of the fructose group. All rats were sacrificed at week 16 with liver biopsies collected and stored for approximately 1 year prior to this project. In this project, Hematoxylin and Eosin (H&E) staining, Picro Sirius Red (PSR) staining, and Oil Red O (ORO) staining were performed on liver sections collected from these biopsies. A triglyceride assay was used to quantify the triglyceride content in the livers, and reverse transcription quantitative polymerase chain reaction (RT-qPCR) was used to look at differences in gene expression related to inter-organ crosstalk, fatty acid metabolism, cellular stress, inflammation, and fibrosis.

Results: The amount of macrovesicular and microvesicular hepatic steatosis, lipid droplets, and triglyceride content were significantly higher in the fructose group compared to the controls although there was no difference in liver collagen deposition between the groups. mRNA levels of *Atf4* and *Fgf21,* related to cellular stress and possibly inter-organ crosstalk, was upregulated in the fructose group, whereas *Pdk4*, important for fine-tuning the balance between glucose and fatty acid metabolism, was downregulated.

Conclusion: The results from this master's project show that chronic consumption of a 15% fructose solution alters liver metabolism and increases hepatic steatosis but does not induce collagen deposition.

1 Introduction

1.1 Fructose Consumption in the Modern Diet

Fructose is a six-carbon monosaccharide found naturally in fruits, honey, and some vegetables (1). It belongs to the broader category of simple sugars (mono- and disaccharides) and shares the same molecular formula as glucose ($C_6H_{12}O_6$). The difference between fructose and glucose is that fructose contains a ketone group in its structure instead of an aldehyde group. This subtle difference in chemical structure could potentially make fructose, at least under certain conditions, more detrimental to human health than glucose (2).

Fructose is sometimes used as a replacement for glucose and sucrose in processed foods and beverages due to its sweeter taste and smaller glycaemic effect (3,4). However, fructose is mostly consumed as sucrose, or high-fructose corn syrup (HFCS) in the USA (5). In sucrose, fructose is linked to glucose via a glycosidic bond that must be broken by sucrase, whereas in HFCS the fructose and glucose exists in a free form within the syrup (6). However, they have a similar metabolic effect (7).

The main source of added sugars in the modern diet is sugar-sweetened beverages (SSBs), encompassing flavored soft drinks, sports and energy beverages, and packaged fruit juices. It is estimated that approximately 15-17% of the total daily energy intake in western countries is derived from added sugars, with half of this being fructose (8).

Since the mid-twentieth century, there has been a notable shift in the dietary patterns of western countries. Traditional diets, predominantly consisting of unprocessed and minimally processed foods, have largely been supplanted by highly processed, energy-dense foods that are rich in fat, salt, and added sugars (8,9). This transition in dietary patterns is also observed in modern low- and middle-income countries as they increase in prosperity, a phenomenon referred to as the nutrition transition (10,11).

Epidemiological and experimental evidence, supported by plausible mechanisms, suggests that chronic high fructose consumption is linked to fatty liver disease, dyslipidemia, insulin resistance, hyperuricemia, and cardiovascular disease (12,13). However, the detrimental effects of high fructose consumption in the context of a nutritious, energy-balanced diet still remains a controversial topic (2,14,15).

1.2 Fatty Liver Disease and Metabolic Dysfunction

1.2.1 Fructose metabolism

As mentioned, fructose and glucose have the same molecular formula, but with a subtle difference in their chemical structure. This means that there are some similarities regarding their absorption and metabolism, but they are ultimately metabolised through slightly different pathways – with fructose metabolism (fructolysis) being less tightly regulated than glucose metabolism (glycolysis) (16).

Fructose is passively absorbed in the small intestine by transport proteins known as GLUT5 that are located on the apical side of the enterocytes, and is exported to the bloodsteam on the basolateral side by GLUT2 (17). Within the cytoplasm of enterocytes, fructose undergoes fructolysis. Initially, fructose is phosphorylated by fructokinase into fructose-1-phosphate, which is subsequently cleaved by aldolase B into dihydroxyacetone phosphate (DHAP) and glyceraldehyde (GA). GA is then phosphorylated into glyceraldehyde-3-phosphate (GA3P) by triose kinase. At this stage, fructolysis and glycolysis has converged as both DHAP and GA3P are glycolytic products (15).

Approximately 90% of fructose is cleared by the small intestine when only small doses are consumed (< 1g/kg), but at high doses (≥1g/kg) its absorption and clearance capacity is overwhelmed (18). The fructose that is not metabolised in the small intestinte is transported to the bloodstream via GLUT2 transport proteins on the basolateral side of the enterocytes, travels to the liver via the hepatic portal vein, where it too undergoes fructolysis (18). The liver metabolises the majority of fructose in the bloodstream (approximately 55%–71%), with the remainder metabolised by the kidneys (<20%), muscle, and other extrahepatic tissues (16,19).

The key difference between fructolysis and glycolysis is that the allosteric enzyme phosphofructokinase-1 (PFK-1) in glycolysis is regulated by a negative feedback mechanism when intracellular levels of citrate and ATP increase (20). This lack of regulation in fructolysis means that high fructose consumption can result in a rapid depletion of ATP, accumulation of AMP, and an increase in GA3P and DHAP levels, promoting intrahepatic triglyceride synthesis and storage, and uric acid production (12).

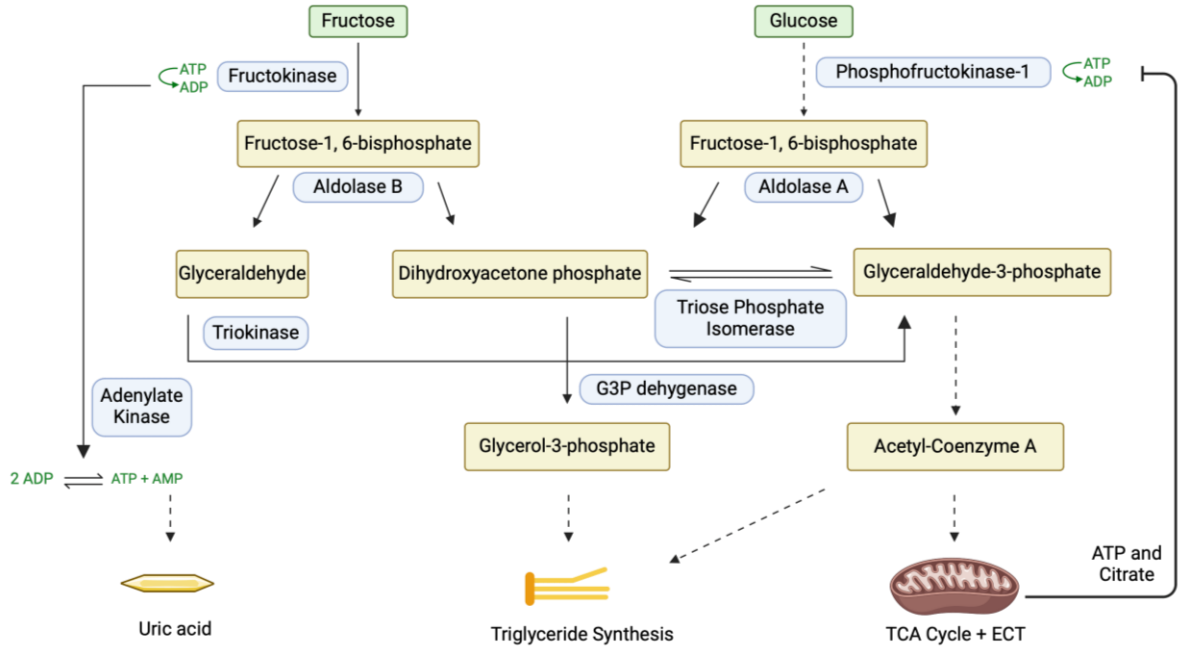

Figure 1 Schematic overview and comparison of fructolysis and glycolysis. Glycolysis is regulated at step three (phosphofructokinase-1) by ATP and Citrate, whereas fructose is not subject to this regulation. Fructolysis promotes triglyceride synthesis by increasing the availability of glucogenic products (glyceraldehyde-3-phosphate and dihodroxyacetone phosphate) and increase uric acid production by increasing AMP accumulation. Figure made with BioRender. Adapted from Lowette et al (15).

1.2.2 Fatty Liver Disease – From NAFLD to MAFLD

Non-alcoholic fatty liver disease (NAFLD) is a term introduced in the 1980s by Schaffner and Thaler, describing liver fat accumulation not caused by heavy alcohol use or other liver disease (21). Affecting about 25% of the global population, or roughly 2 billion people, NAFLD's prevalence exceeds that of obesity and type 2 diabetes combined (22–24).

Initially, NAFLD was viewed solely as the liver manifestation of the metabolic syndrome (MetS). MetS is a condition characterized by the clustering of at least three of five components: abdominal obesity, elevated triglycerides, low HDL-C, hypertension, and elevated fasting glucose. However, accumulating evidence suggests an alternative connection between NAFLD and MetS, with MetS possibly originating in the liver (25).

In 2020, a panel of experts from 22 countries proposed changing the NAFLD nomenclature to metabolic dysfunction-associated fatty liver disease (MAFLD) (26–28). They also

recommended new diagnostic criteria that would better reflect current understanding of the disease. The primary distinction is that MAFLD diagnosis relies on the presence of hepatic steatosis alongside overweight or obesity, type 2 diabetes, or a normal BMI combined with at least two metabolic abnormalities, without any exclusion criteria (29). This change aims to recognize the disease's varied nature and move away from the stigma of alcoholism. It could also offer a more effective way for clinicians to identify patients at risk of long-term metabolic issues (30,31). Due to the novelty of the MAFLD nomenclature, the terms MAFLD and NAFLD may be used interchangeably in this master's thesis.

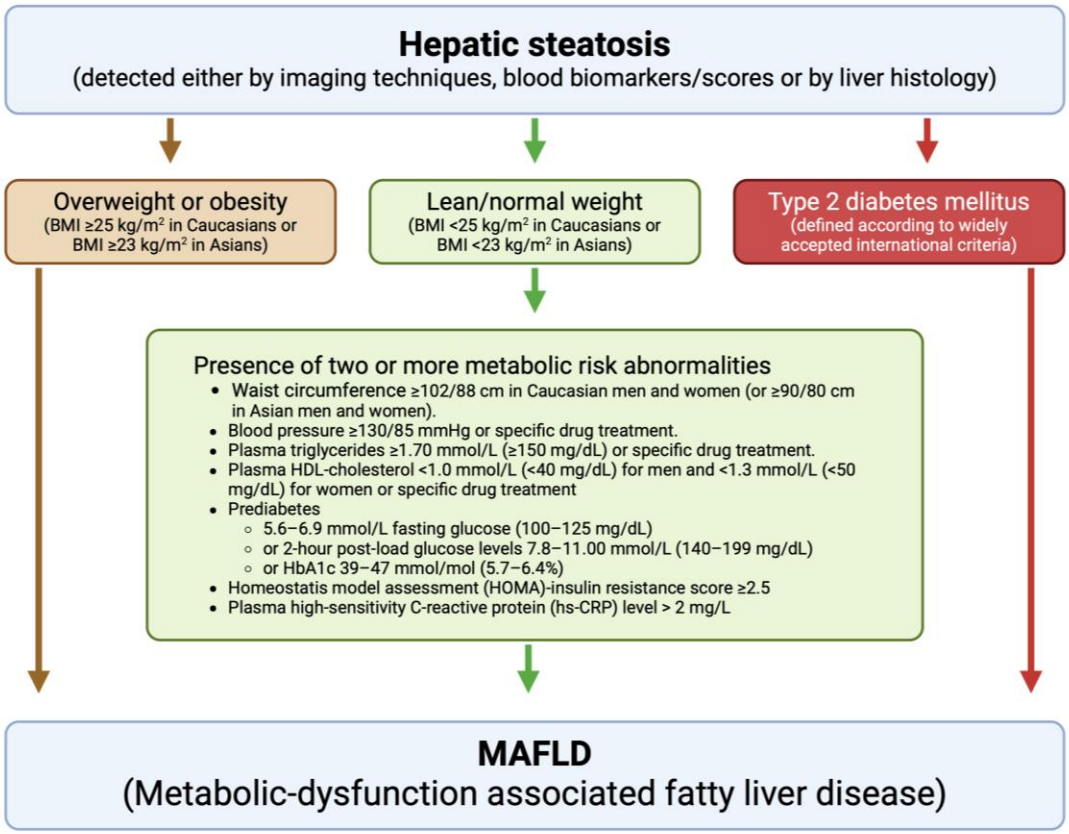

Figure 2 MAFLD diagnostic criteria. Diagnosis of MAFLD is based on the presence of hepatic steatosis combined with either overweight/obesity, type 2 diabetes, or a normal body weight with at least two metabolic abnormalities (waist circumference, hypertension, elevated plasma triglyceride, low HDL-cholesterol, prediabetes, insulin resistance, inflammation). Thus, it is a disease based on inclusion criteria rather than exclusion criteria. Figure made with BioRender. Adapted from Eslam et al (27).

1.3 Liver Physiology and Metabolism in Health and Disease

1.3.1 Anatomy and Blood Supply

The liver is located in the upper right corner of the abdominal cavity and is the largest internal organ in the human body. It receives blood from two distinct sources – the hepatic artery transporting oxygenated blood from the heart, and the hepatic portal vein transporting deoxygenated yet nutrient rich blood from the digestive system. Approximately 25–30% of the total cardiac output flows through the liver (1500 ml/min at rest), and about 70% of this blood is received from the portal vein (32).

The venous linkage between the capillaries of the digestive system and the liver is known as the hepatic portal system. The hepatic portal system is part of the larger splanchnic circulation, which encompasses the arterial blood flow originating from the aorta and coursing through all of the internal organs, before ultimately being drained into the inferior vena cava (33).

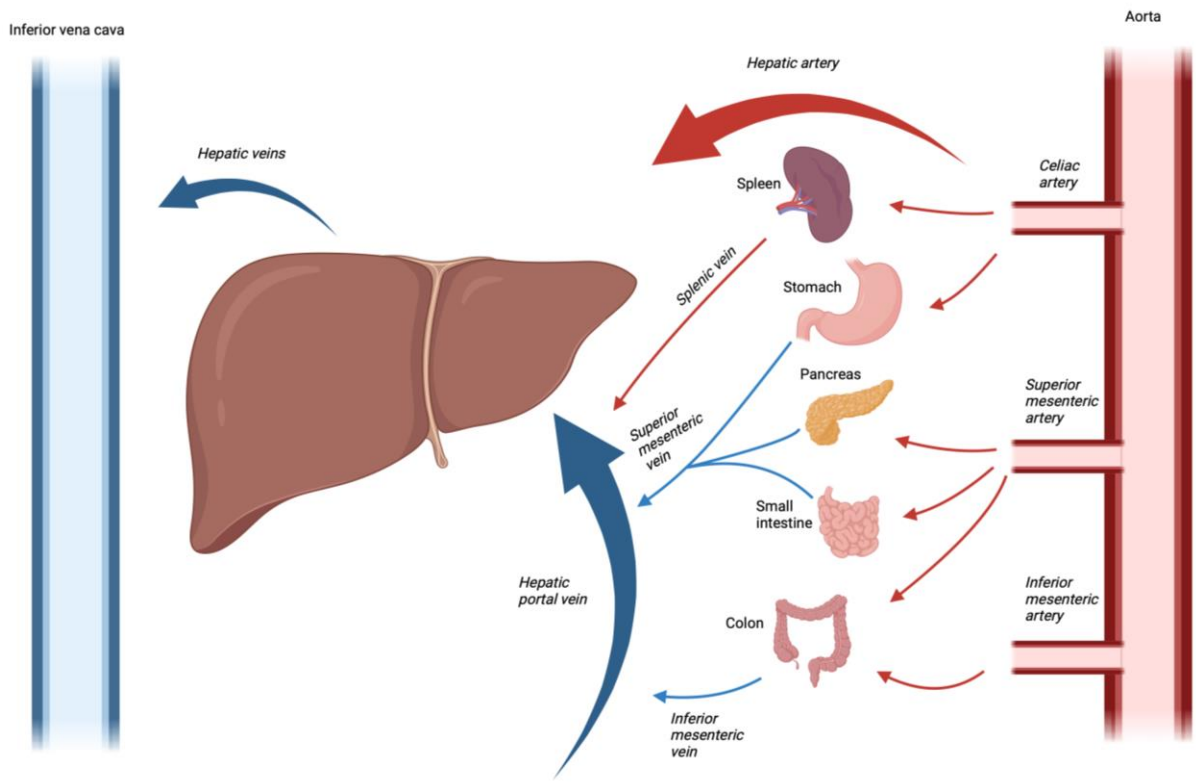

Figure 3 Splanchnic circulation and the hepatic portal system. The hepatic portal system is a part of the larger splanchnic circulation. The liver receives nutrient rich blood from the hepatic portal vein and oxygen rich blood from the hepatic artery. Figure made with BioRender. Adapted from Gelman et al (33).

The liver acts as an important hub for processing nutrients and other substances before distributing them throughout the body, often referred to as the first-pass effect (34). This intricate processing occurs within the liver lobules which are the smallest functional units of the liver. Each lobule has a hexagonal structure, and at every corner is a collection of three different branches – an artery, a vein, and a bile duct – known as a portal triad. The vein and artery of the portal triad converges into a specialized type of capillary known as a sinusoid (35). The endothelium of the sinusoids have large pores between them called fenestrae, allowing for an easy exchange of nutrients and substances between the blood and the hepatocytes. From the portal triads and down towards the central vein, the area between two sinusoids can be further subdivided into zones 1, 2, and 3, with each zone having different functions (36).

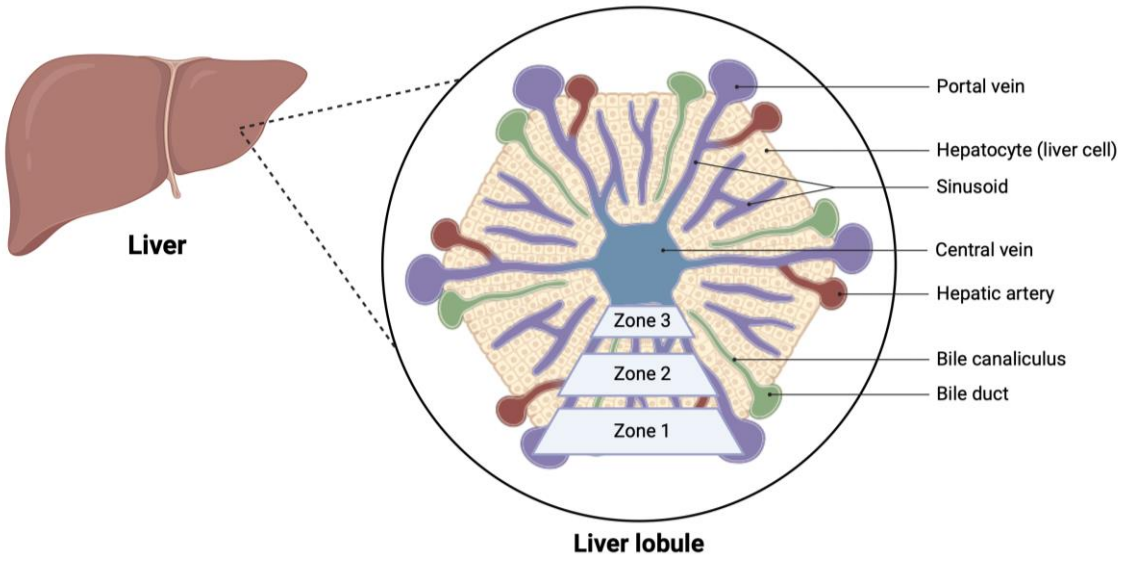

Figure 4 Anatomy of the liver lobule. The liver lobules have a hexagonal structure and are the smallest functional units of the liver. They can be divided into different zones. Zone 1 (the periportal zone) is closest to the portal triads and therefore receives the most oxygenated and nutrient rich blood from the hepatic arteries and veins. Hepatocytes in this zone are mainly involved in gluconeogenesis, glycogenolysis, and production of urea. Zone 2 (the midzonal zone) is mainly involved in glycolysis, fatty acid oxidation, and xenobiotic metabolism – the metabolism of foreign substances including drugs, food additives or other exogenous compounds. Zone 3 (the pericentral zone) is closest to the central vein and the blood in this area is relatively oxygen and nutrient poor compared to zone 1. The hepatocytes in zone 3 have a higher amount of the enzyme xanthine oxidase in their cytoplasm, which is the enzyme required to produce uric acid from the breakdown of purines. Figure made with BioRender. Adapted from Campbell (32).

Zooming closer into a liver sinusoid, we can see that between the endothelial cells and hepatocytes is a thin perisinusoidal area known as the space of Disse (37). The space of Disse contains a type of cell known as hepatic stellate cells (HSCs) or Ito cells, which make up 5–8% of the total number of livers cells (38). In the normal liver, HSCs exists in a quiescent state where their main role is to produce and maintain the basal extracellular matrix, store fat and vitamin A (as retinyl esters), produce growth factors and cytokines, and present antigens to the cells of the innate immune system (39). On the luminal side of the sinusoids are resident macrophages known as Kuppfer cells and natural killer cells known as Pit cells, both of which are part of the innate immune system (40). In response to liver injury and inflammation (caused by, for example, enlarged and damaged hepatocytes), Kupffer cells are activated, and they in turn cause the HSCs to go from their quiescent state to an active state where they begin to proliferate and secrete collagen and other extracellular matrix proteins (41).

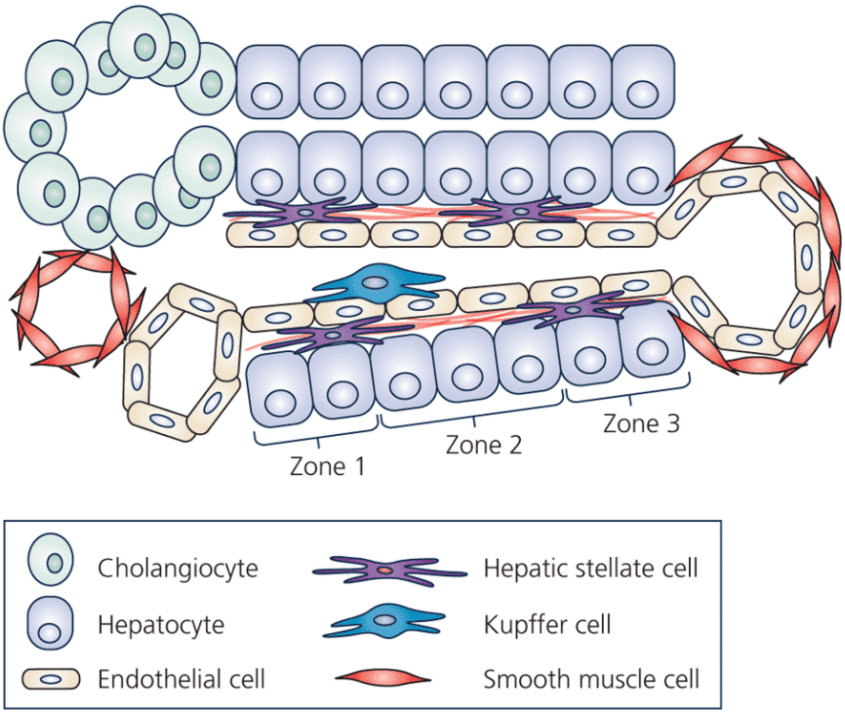

Figure 5 Cross-sectional illustration of a liver sinusoid. On the inside of the sinusoids are macrophages known as Kupffer cells (represented as a blue cell). Not represented are natural killer cells known as Pit cells, but they are also located inside the sinusoids. In the space of Disse between the endothelial cells and hepatocytes are hepatic stellate cells. Image from Kamm and McCommis (2022) (39).

1.3.2 Short-Term and Long-Term Metabolic Regulation

Metabolism is the branch of biochemistry that focuses on the complex series of chemical reactions (metabolic pathways) occurring within living organisms to sustain life (42). Metabolism can be broadly divided into catabolism and anabolism. Catabolism encompasses the metabolic pathways that facilitate the breakdown of complex molecules into simpler, smaller units. This includes the breakdown of carbohydrates to glucose, triglycerides to free fatty acids and glycerol, and proteins to amino acids. Conversely, anabolism comprises the metabolic pathways responsible for constructing larger and more complex molecules from these simpler units. This includes glycogen synthesis from glucose, triglyceride synthesis from fatty acids and glycerol, and protein synthesis from amino acids (43,44).

In the short term, metabolism is regulated by hormones, mainly insulin and glucagon (from a liver centric perspective) which are released from the pancreas and transported to the liver in response to feeding or fasting conditions (43). Insulin promotes energy storage and nutrient uptake, while glucagon stimulates energy mobilization. In the long term, metabolism can adapt to various physiological states and nutrient availabilities through changes in gene expression (44,45). This adaptability is crucial for maintaining homeostasis and overall health.

Gene expression consists of transcription and translation, both of which contain an initiation, elongation, and termination phase (46). Transcription occurs in the cell nucleus and is the process in which the information stored in a DNA sequence is transcribed into a complementary RNA molecule by RNA polymerase (46). Once transcribed, the RNA molecule undergoes a post-transcriptional modification to produce a mature messenger RNA (mRNA). Translation is the process in which mRNA is used for protein synthesis (47). The mRNA is transported out of the nucleus and into the cytoplasm, binds to a ribosome, and is decoded to produce a sequence of amino acids. During translation, transfer RNA (tRNA) molecules deliver amino acids to the ribosome, where they are assembled into a polypeptide chain according to the mRNA's nucleotide sequence. Post-translational modifications of proteins can occur during or after synthesis, and involves enzyme-mediated addition of functional groups to the proteins (48).

Gene expression can be regulated at the transcriptional, post-transcriptional, translational, and post-translation level, with regulation at the transcriptional level being most common (49–51).

The gene and nomenclature style from the American Society for Clinical Investigation (ASCI) will be used when describing genes (52). This includes italicization of gene symbols, genotypes, mRNAs and cDNAs, but not gene names, gene products and phenotypes, as well as no capitalization of gene and protein symbols from rats and mice.

1.3.3 MAFLD, Inter-Organ Crosstalk and Heart Failure

Metabolic-dysfunction loosely refers to the presence of at least one MetS component and can occur due to a number of lifestyle-related risk factors, including overconsumption of calories (which include high fructose and/or fat intake), obesity, insulin resistance, sedentary lifestyle, and alcohol intake (53). In response to these risk factors, alterations in gene expression can occur within cells, including hepatocytes, reflecting an array of physiological adaptations and dysregulations such as fatty liver disease (54,55). Notably, expression of genes implicated in inflammation, oxidative stress, lipid metabolism, carbohydrate metabolism, insulin signalling, and fibrosis are likely to be affected (41,54,55). This intricate interplay of genetic responses underscores the multifaceted nature of metabolic dysfunction in the liver, illustrating the complex mechanisms by which lifestyle factors can impact liver health and function.

Accumulation of excess triglycerides in the hepatocytes, stored in vesicles called lipid droplets, is the hallmark of MAFLD. In patients with MAFLD approximately 60% of the fatty acids used to synthesize triglycerides originate from free fatty acids (FFA) released from adipose tissue, 25% originate from hepatic de novo lipogenesis (DNL), and 15% arise from dietary fatty acids transported by chylomicrons (CM) (56). β-oxidation and VLDL production and secretion in the liver is also increased during MAFLD, but these compensatory mechanisms are insufficient in the face of overwhelming levels of fatty acids from FFA, DNL, and CMs (41).

NAFLD exists on a spectrum with overlapping stages. Non-alcoholic fatty liver (NAFL) is the first stage of NAFLD/MAFLD and is defined as an accumulation of fat (steatosis) in >5% of hepatocytes (25). The next stage is non-alcoholic steatohepatitis (NASH) which is characterized by NAFL combined with inflammation, ballooning of hepatocytes, and fibrosis. The exact mechanisms of the transition from NAFL to NASH are not completely understood, but it is believed to be related to the increase in size of the hepatocyte lipid droplets from microvesicles to macrovesicles, culminating in the destruction of the macrovesicles and an

inflammatory response to this injury which include activation of HSCs (41). The final stage of NAFLD/MAFLD is cirrhosis, which occurs when the liver has been irreversibly damaged due to a high degree of fibrosis (57). In the early stages of cirrhosis, the liver can still perform its vital functions, but disease progression will eventually result in decompensated cirrhosis where this is no longer possible (58).

During cirrhosis, a complication known as portal hypertension (PH) will occur. The pressure difference between the hepatic portal vein and the inferior vena cava is called the hepatic venous pressure gradient (HVPG) (58). The HVPG is normally less than or equal to 5 mmHg, but when the liver is injured this pressure difference becomes higher and a difference of 10 mmHg is considered clinically significant PH (59). This in turn will increase the risk of other complications such as ascites, variceal bleeding, hepatic encephalopathy, and even multi-organ failure (58).

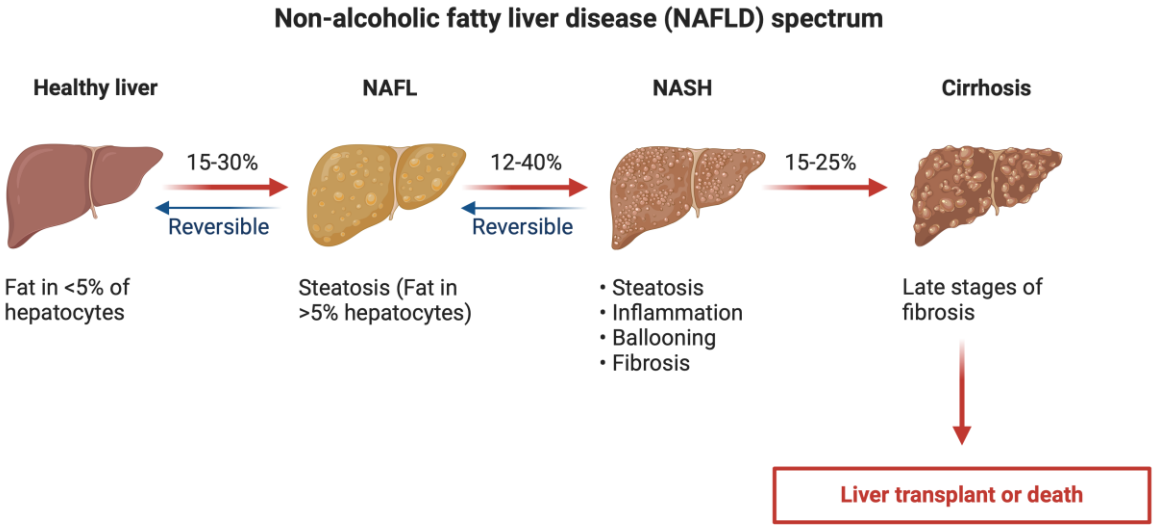

Figure 6 The spectrum of NAFLD. NAFL is defined as >5% fat in the liver and is considered reversible up to a certain stage. When NAFL is combined with inflammation, ballooning of hepatocytes, and/or fibrosis, is has progressed to NASH. When the fibrosis reaches a certain threshold, the liver will be permanently damaged, resulting in cirrhosis. Premade figure from the BioRender template library.

As the liver plays an important role in sensing and responding to nutrient availability, it is therefore an important regulator of systemic energy homeostasis. It can communicate with the

central nervous system, adipose tissue, pancreas, heart, and skeletal muscle through the secretion of liver-derived factors (proteins and peptides) referred to as hepatokines (60). These organs can also communicate with the liver and with each other through their own signalling molecules, and this is referred to as inter-organ crosstalk (61).

MAFLD is increasingly being recognized not only as the liver manifestation of MetS, but as a multisystem disease in its own right, able to affect extra-hepatic organs such as the heart (62). It has been hypothesized that there is a pathophysiological continuum between MAFLD and heart failure with preserved ejection fraction (HFpEF) – also described as a multisystem disease – that is in part mediated by proinflammatory signaling molecules such as interleukin 6 (IL-6) and tumor necrosis factor alpha (TNF-α) (63). Due to also sharing many co-morbidities such as cancer, T2DM, kidney disease, and obesity, it has been suggested that MAFLD be considered as an emerging risk factor for HFpEF complications.

In patients with HFpEF it has also been found that plasma levels of fibroblast growth factor 21 (FGF21) is increased (64). FGF21, a type of peptide hormone with anti-inflammatory properties, is sometimes referred to as a hepatokine due to mainly being released from the liver. It is released in response to nutritional and metabolic challenges such as starvation or prolonged fasting, a ketogenic diet, alcohol consumption, amino acid restriction and excess sugars (65). FGF21 can bind to the FGF receptor 1c (FGFR1c) and its co-receptor β-klotho (Klb) in the heart, where its role has been hypothesized to be suppression of inflammation and protection against adverse cardiac remodeling during heart failure (64,66).

1.3.4 MAFLD and Gene Expression

As stated in section 1.3.2, gene expression can be regulated at the transcriptional, post-transcriptional, translational, and post-translation level, with regulation at the transcriptional level being most common (49–51). Transcriptional regulation requires proteins known as transcription factors that bind to specific regions of the DNA, which in turn promotes or inhibits expression of particular genes in these regions (49). Lipid homeostasis in the liver is mainly regulated by transcription factors known as sterol regulatory element binding protein 1c (SREBP-1c) and peroxisome proliferator-activated receptors (PPARs), whereas the hepatic connection between lipid and glucose metabolism is mediated by the carbohydrate-responsive element-binding protein (ChREBP) (67).

ChREBP (also known as MondoB) belongs to a family of transcription factors known as the Mondo family (68). It was initally considered a glucose sensor, but it is now recognized that it senses other dietary sugars including fructose (fructose especially activate the ChREBPβ isoform) (68,69). ChREBP regulates the expression of genes involved in NAFLD through activation of de novo lipogenesis, and thus has a complex and interconnected relation to SREBP1-c (68).

SREBP-1c belongs to a family of transcription factors known as the basic-helix-loop-helix-leucine zipper (bHLH-LZ) family, along with its two isoforms SREBP-1a and SREBP-2 that are involved in cholesterol synthesis (70). SREBP-1c is regulated by nutritional status and high insulin levels, and regulates the expression of genes involved in fatty acid synthesis (71).

The PPARs are a superfamily of nuclear transcription factors involved in metabolism, inflammation, and oxidative stress (72). In the liver, PPARα is activated by binding to fatty acids and promotes fat oxidation and thermogenesis (73). PPARγ promotes de novo lipogenesis and adipogenesis (74). The peroxisome proliferator-activated receptor gamma coactivator 1-alpha (PPARGC1) can activate PPARα and PPARγ (75).

Closely related to PPARα is carnitine palmitoyl transferase-1 (CPT1) which is encoded by the the *mCPT1* gene (73). CPT1 is an essential enzyme in mitochondrial β-oxidation because it catalyzes the transfer of fatty acyls from acetyl coenzyme-A to carnitine, allowing them to be transported from the cytosol and into the mitochondrial matrix through the outer mitochondrial membrane (73). Reduced *mCPT1* expression is associated with increased liver triglycerides (76,77).

Also related to fatty acid metabolism is pyruvate dehydrogenase kinase 4 (PDK4) which shifts metabolism from glucose oxidation to fat oxidation by inhibiting the activity of the pyruvate dehydrogenase complex (PDC). PDC connects glycolysis to the citric acid cycle by converting pyruvate into acetyl-CoA, and inhibition of PDC therefore leads to an accumulation of pyruvate in the cytosol and forces a shift towards fat oxidation by the mitochondria (78). PDK4 deficiency has been shown to improve glucose tolerance, which makes sense considering that a lack of PDK4 should improve glucose oxidation (79).

Another feature of fatty liver disease is inflammation, and the pro-inflammatory cytokines interleukin-6 (IL-6) and tumor necrosis factor-α (TNF-α) are significantly associated with NAFLD (80). Both IL-6 and TNF-α has been shown to promote hepatic insulin resistance through the JNK signaling pathway, and IL-6 has also been shown to activate hepatic stellate cells (HSCs) which in turn promotes collagen synthesis (fibrosis) (81). Activated HSCs also increase expression of the collagen genes, *Col1a1* and *Col3a1*, which regulate the production of collagen types I and III, respectively. Collagen type III is more elastic and more common during the early stages of NAFLD, with the stiffer type I collagen taking over as the fibrosis worsens (82).

Due to the large amount of protein synthesis in the liver, the hepatocytes are rich in ER (endplasmic reticulum). During NAFLD, a protective pathway known as the UPR (unfolded protein response) is activated. ATF4 (activating transcription factor 4) and CHOP (C/EBP homologous protein) are downstream proteins activated by UPR, and are involved in protein folding, autophagy, redox reactions, amino acid metabolism and apoptosis (83,84).

1.4 A Translational Study

1.4.1 Background

In order to elucidate the role of fructose in the development fatty liver disease, hypertensive heart disease, and potentially neurodegenerative disease, a translational study focusing on inter-organ crosstalk between the liver, heart and brain is being conducted by the Cardiovascular Research Group at the Department of Medical Biology (IMB), UiT The Arctic University of Norway.

The main hypothesis of this translational study is that chronic high-fructose consumption leads to fatty liver disease, hypertension, cardiac remodeling, and cognitive decline. To test this hypothesis and to understand the underlying mechanisms, an experimental rat model will be used to promote fructose-induced metabolic dysfunction in Sprague-Dawley rats.

The experimental rat model will lay the groundwork for translation through future epidemiological and experimental studies including dietary interventions and the role of FGF21 in human disease. This master's project has been conducted as a part of this experimental phase, and will be focusing on the histological, biochemical, and genetic effects of chronic high-fructose consumption in male Sprague-Dawley rats.

1.4.2 Experimental Rat Model

Using high-fructose feeding to induce fatty liver disease and metabolic dysfunction in rats is an established experimental model. However, protocols also vary widely in regard to duration, concentration, and method of nutrient delivery.

In a systematic review and meta-analysis by Toop and Gentili it has been demonstrated that ad-libitum diets supplied with a 10–21% fructose drink is associated with elevated circulating glucose and lipids, and increased triglyceride production and accumulation in the liver (85). These concentrations are also considered to be physiologically relevant to humans, as opposed to high-fructose diets containing 60% fructose drinks or higher.

A study by Meng et al (2016) treated rats with a 15% fructose drink and reported this to be equivalent to approximately 130 g of daily sugar intake in 1–2L soda drinks in a human weighing 60 kg (86).

Based on these findings, an experimental rat model of chronic high-fructose intake was made by administering fructose to drinking water to create a 15% fructose solution.

Although the fructose content in soft drinks and fruit juices available to humans is around 5-7% it should be noted that the purpose is not to completely mimic the fructose content of an average human diet in this study. Instead, fructose has been selected as a target nutrient that will be administered in a sufficient concentration such that histological, biochemical, and gene-expression changes can be detected at the organ level while other factors are controlled. This is a cost-effective treatment, well-tolerated by the animals, and the fructose concentration is still kept within a reasonable physiological range.

1.5 Aims of this Investigation

The aim of this master's project is to investigate the effects of a 16-week high fructose intervention on liver histology, triglyceride content, and gene expression in male Sprague-Dawley rats. More specifically, the hypothesis' being tested are:

1) Is there a difference in liver histology between the fructose and control group as measured by three different staining methods?
2) Is there a difference in liver triglyceride content between the fructose and control group as measured by colorimetry?
3) Is there a difference in expression of genes involved in fatty acid metabolism, fibrosis, cellular stress, inflammation and FGF21 between the fructose and control group as measured by RT-qPCR

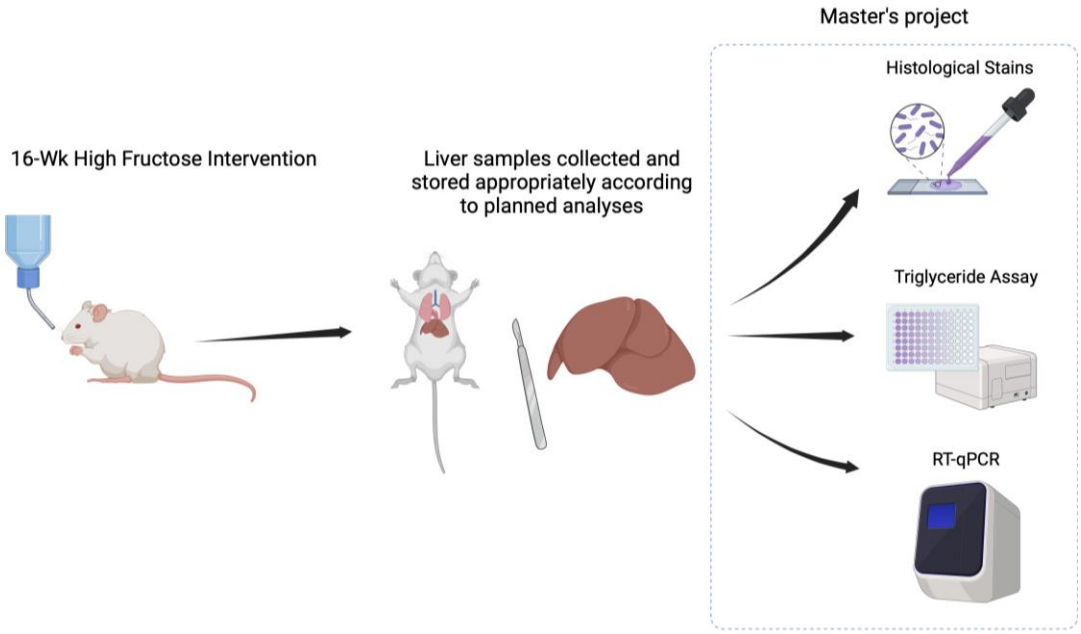

Figure 7 Scope of the current master's project. This master's project is a part of the experimental phase of a larger translational study. Male Sprague-Dawley rats have previously been sacrificed after a 16-week high fructose intervention, and investigation of the livers from these rats will be the focus of this project.

2 Materials and Methods

2.1 Animals and Diets

All data for this master's thesis was collected from animals that had already been sacrificed as part of an ongoing project approved by the Norwegian Food Authorities (Mattilsynet) and the Unit of Comparative Medicine at UiT The Arctic University of Norway (FOTS ID 28063).

Sprague-Dawley rats, aged 10-12 weeks at arrival, were obtained from Janvier Laboratories in France. After one week of acclimatization, 32 male rats were randomized into an intervention group and a control group. Both groups were given ad-libitum access to a standard chow diet and drinking water, with 15% fructose administered to the drinking water of the intervention group for a total of 16 weeks. The standard chow diet contained 67 E% from carbohydrates, 24 E% from proteins, and 9 E% from fats.

There were two rats in each cage and body weight was measured at regular time intervals, approximately 2-3 throughout the course of 16 weeks (Figure 6). In addition, body composition was obtained using Echo MRI. Rats (awake) were placed in a specialized tube that was inserted into the EchoMRI and scanned using nuclear magnetic resonance that enhances the contrast between fat, lean and free water and allows for body mass analysis. The measurements last between 2-3 minutes in total and is safe for the animals.

Blood pressure was obtained non-invasively in conscious rats by tail-cuff measurements in both groups at 3 timepoints throughout the study (CODA- Kent Scientific). Rats underwent tail-cuff measurements on 2 consecutive days where day 1 was for acclimatization and the final measurements were obtained on day 2. Other In-vivo procedures including blood samples, and two memory tests, were also performed although these results are not included in the present thesis.

The trial lasted for 16 weeks in total, with one rat each from the control and intervention group being euthanized at week 6, 8, 12 and 14. All remaining rats were euthanized at week 16 (n = 24). Liver biopsies were collected and stored appropriately according to planned analyses. The rats that were euthanized before week 16 (n = 8) are not included in this project.

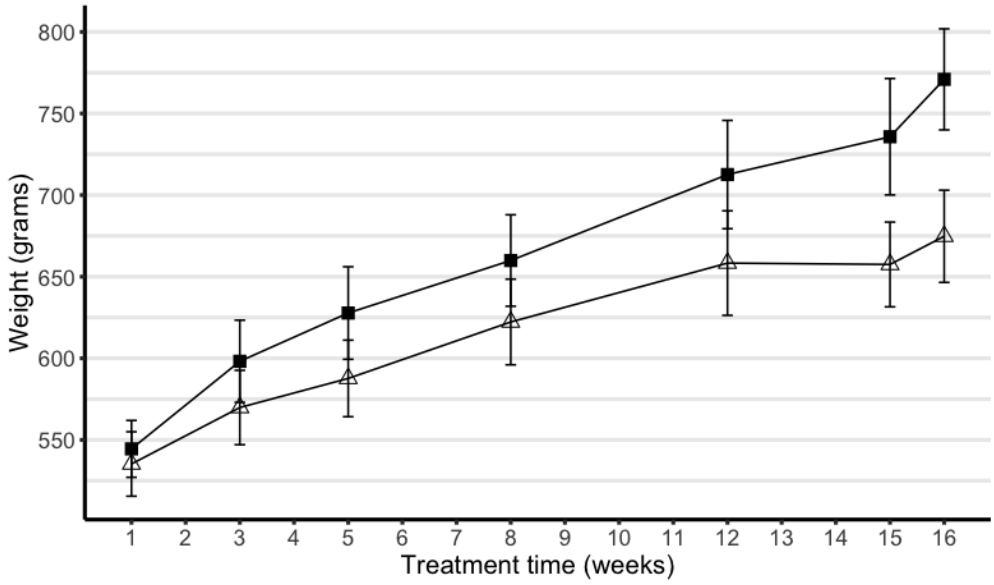

Figure 8 Weight change over treatment time in weeks. Changes in mean body weight during the 16-week intervention with error bars showing the standard deviations. This initial data support that the fructose intervention was having an effect.

2.2 Histological Analysis

2.2.1 Preparation and Sectioning

Formalin-fixed, paraffin-embedded blocks of liver tissue (n = 24) had been stored at room temperature for approximately one year prior to the start of this master's project. Each block was cut in the sagittal plane into 5 µm sections using a cool-cut rotary microtome (Microm HM355S, Epredia) with low profile blades (MX35 Ultra Microtome Blade, Epredia). Each section was collected in a lukewarm water bath, placed on a 1 mm thick microscope slide (SuperFrost, Menzel- Gläser), and dried at room temperature. 48 slides were made from the microtome (2 x 24).

Similarly to the paraffin-embedded blocks, an equal number of OCT-embedded (optimal cutting temperature) blocks of liver tissue had been stored in a freezer at -70 °C. Each OCT-embedded block was cut into 10 μm sections in the sagittal plane but using a cryostat instead of a microtome (CryoStar NX70). The low profile blades used during the microtome sectioning was cooled down to -25 °C and the OCT block-holder was cooled down to -15 °C. All cryosections were placed on a 1 mm thick microscope slide and stored again at -70 °C. 24 slides were made from the cryostat.

2.2.2 Hematoxylin and Eosin Staining

Hematoxylin and eosin (H&E) staining is one of the most commonly used staining techniques in histopathology due to its simplicity, price, and versatility. Hematoxylin gives a purple-blue color to the cell nuclei, and the eosin gives different shades of pink to the contents of the cytoplasm and extracellular matrix (87). The color contrast between hematoxylin and eosin provides a detailed overview of tissue architecture and plays a crucial role in the screening of MAFLD by allowing for the visual assessment of the severity of hepatic steatosis. Equipment:

- Hematoxylin Harris, 1L (Chemi-Teknik AS, Norway)
- Eosin Y-solution 0.5% alcoholic, 500 mL (Sigma Aldrich, Germany)
- Xylene, 1L (VWR Chemicals, France)
- Double-distilled water (ddH_2O)
- 70/96/100% ethanol, 1L (VWR Chemicals, France)
- Sodium bicarbonate ($NaHCO_3$), 1 kg (Sigma-Aldrich, Germany)
- Magnesium sulphate ($MgSO_4$), 1 kg (Sigma-Aldrich, Germany)
- Histokitt (GlaswarenFabrik Karl Hecht, Germany)

In preparation for H&E staining, staining jars were filled with xylene, ethanol, ddH_2O, Harris Hematoxylin, Scott's Solution, and Eosin. Xylene is an aromatic hydrocarbon that is widely used as a dewaxing and clearing agent in histology, but due to its toxicity it was important to work in a fume hood and wear a lab coat and nitrile gloves for safety (88). Scott's solution (Scotts Tap Water) is a type of water solution that can enhance the quality of the hematoxylin stain and was made by mixing together 1 litre of ddH_2O with 3.5 g sodium bicarbonate ($NaHCO_3$) and 20 g magnesium sulphate ($MgSO_4$).

The first step of H&E-staining is to deparaffinize and rehydrate all slides. All slides were set up in a rack and put through two changes (jars) of xylene for 10 minutes each. The rack was then put through two changes of 100% ethanol for 5 minutes each, one change of 96% ethanol for 5 minutes, one change of 70% ethanol for 5 minutes, and a change of ddH_2O for 2 minutes. This deparaffinization and rehydration process makes the tissue penetrable by other aqueous solutions.

The rack was then put in a change of Harris hematoxylin for 15 minutes, followed by a change of ddH_2O for 2 minutes, and a change of Scott's solution for 2 minutes. A change of 96% ethanol was then used for 2 minutes before proceeding to a change of eosin for 30 seconds. Following this, a change of 96% ethanol was used for 1 minute and two changes of 100% ethanol was used for 1 minute each, before finally using two changes of xylene for 2 minutes each to clear the slides (making them more transparent). All slides were mounted with histokitt before applying a cover glass.

2.2.3 Picro Sirius Red Staining

Picro Sirius Red (PSR) is a dye containing negatively charged sulfonate groups that can bind with positively charged amino groups in collagen fibers, giving the fibers a red color. In a brightfield microscope, this can be observed as red fibers on a yellow background. The Picro Sirius Red Stain Kit from Abcam (ab150681) was used in this project, containing:

- Picro Sirius Red Solution, 250 ml
- Acetic Acid Solution 0.5 %, 2 x 250 ml

Similarly to the H&E-protocol, the PSR-protocol began with deparaffinization and rehydration. 24 slides from the paraffin-embedded blocks of liver tissue were put in a rack and baked overnight at 60 °C. On the following day, the rack was put through 3 changes of xylene for 10 minutes, 2 changes of 100% ethanol for 3 minutes, 1 change of 96% ethanol for 3 minutes, and 1 change of 70% ethanol for 3 minutes. Finally, the rack was put in 1 change of ddH_2O for 3 minutes.

Following the deparaffinization and rehydration, a DAKO pen was used to draw a water repellant circle around the tissue section of each slide and 150 µl of Picrosirius Red Solution

was applied to this circle. The slides were incubated in a glass box at room temperature for 60 minutes.

After the incubation period, all slides were rinsed twice using a plastic pipette and then rinsed again using 100% ethanol. All slides were put back in the and put through 2 changes of 100% ethanol for 1 minute each and two changes of xylene for 30 seconds before being mounted with histokitt and having a cover glass applied.

2.2.4 Oil Red O Staining

Oil Red O (ORO) is a fat-soluble dye which stains lipids but not cell membranes and has been found to be the most accurate method for quantifying fat droplets in both mouse and human liver biopsies (89). The Oil Red O Stain Kit from abcam (AB150678) was used in this project, containing:

- Hematoxylin (Modified Mayer's Solution), 125 mL
- Oil Red O Solution, 1 x 125 mL
- Propylene Glycol, 1 x 500 mL

Cryosections were placed in a slide rack and thawed at room-temperature for more than 30 minutes. The rack was then put through a change of propylene glycol for 5 minutes and then incubated in a change of ORO solution at room-temperature overnight. The next morning, the rack was put through a change of 85% propylene glycol (diluted with ddH_2O) for 1 minute, dipped in 2 changes of ddH_2O, dipped in 1 change of Hematoxylin, and rinsed in tap water and two changes of ddH_2O. All slides were then mounted using an aqueous mounting medium (Mowiol) made by lab engineers are the UiT Advanced Microscopy Core Facility (AMCF) before putting on a cover glass.

2.2.5 Slidescanning

An Olympus VS120 slidescanner, courtesy of the AMCF, was used in order to create high resolution brightfield images of the HE-, PSR-, and ORO stained slides. Prior to scanning, a CSV template file containing the names and staining techniques used was uploaded to the UiT FileZilla server, which could then be accessed on the slidescanner-computer. All slides

were transferred into a cassette according to the sample template and placed into the slide scanner. On the slidescanner-computer, Expert Batch was chosen as the scan mode, and in the scan settings 20x magnification was chosen. A batch scan overview was then performed which took approximately 2 minutes per slide for a total of 144 minutes. After the overview scan was complete, the correct scan area on each slide had to be manually chosen if the autodetect function did not correctly identify the stained sections. After choosing the correct scan area, several focus areas on each sample area had to be chosen. After the scanning was completed, images were stored in the UiT FileZilla server.

2.2.6 Digital Pathology Image Analysis

All images were loaded into QuPath, an open source software for digital pathology image analysis (90). Three squared areas (250000 μm^2 each) was chosen at random by the software. Regions containing blood vessels were excluded – however, a stain vector (color identifier) for the PSR stain was created by zooming into a blood vessel wall and marking a red area. This vector was then used to teach QuPath how to identify the PSR stain, which in turn was used to measure the amount of area stained within each square. For the ORO stain, a similar process was used but the stain vector was made by zooming into a lipid droplet.

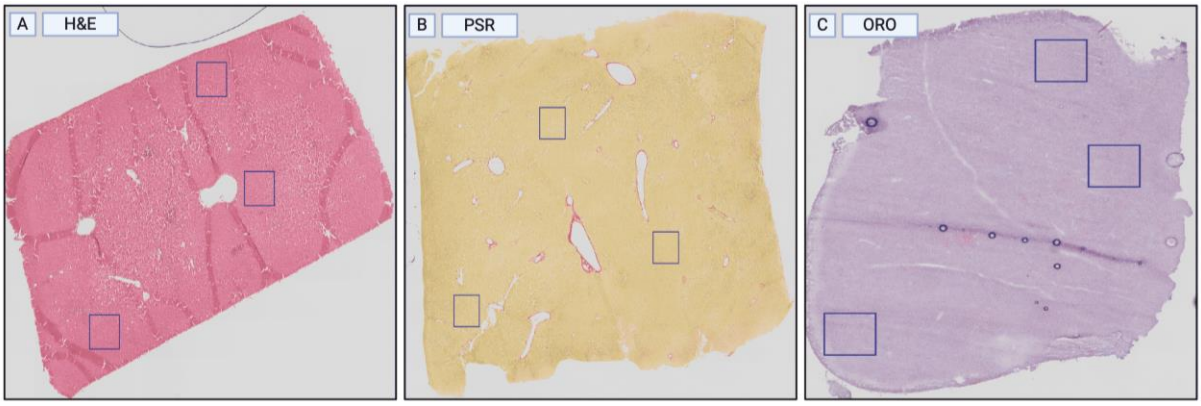

Figure 9 Sample slide overview. All images were loaded into QuPath, and the program was set to choose three random areas covering 250000 μm2 each. Blood vessels were excluded.

Setting stain vectors in QuPath:

1) Zoom in and draw a small rectangle in an area with the stain of interest.

2) Choose *Image* from the left side menu, which contain a list of the names "Stain 1", "Stain 2", "Stain 3".
3) Double click on "Stain 2" and name it "PSR".

After setting the stain vectors, QuPath was used to detect PSR and ORO staining in the three chosen squares of each slide image.

1) In the QuPath top menu, choose *Classify*, *Pixel Classification* and *Create Thresholder*. The Thresholder menu will open. Name it "PSR Threshold", use the following settings, then close the menu.
    - Resolution – Full
    - Channel: ORO
    - Prefilter: Gaussian
    - Smoothing Sigma: 0
    - Threshold: 0.25 (0.30 for PSR)
    - Above threshold: Positive
    - Below Threshold: Ignore*
    - Region: Any annotation ROI
2) In the top menu, choose *Classify*, *Pixel Classification*, and *Load pixel classifier*. Choose the "PSR Threshold" just created and choose region *Any annotation ROI*.
3) Finally, click *measure* and choose *All annotations*.

The result of this measurement is the square micrometer of area stained by PSR and ORO within the chosen regions of each sample. All measurements were added into an excel document, and as there were 3 regions measured in each sample, the average of these measurements was used when calculating the percentage of area stained in each sample.

$$\frac{\text{Average colored } \mu m^2 \text{ of 3 measurements}}{250000\ \mu m2} \text{ x } 100 = \text{ \% area stained}$$

For H&E staining, a paper on a general NAFLD scoring system for rodent models developed by Liang et al (2014) was used as a visual guide (91). This scoring system looks at the two key features of NAFLD: Steatosis and inflammation. Steatosis is divided into macrovesicular

steatosis, microvesicular steatosis, and hypertrophy. Inflammation is scored by analyzing the number of inflammatory cells per region.

2.3 Triglyceride Quantification

2.3.1 Standard Wells

Colorimetry is an analytical method used to quantify the concentration of a substance by dissolving it in liquid and measuring its absorbance (i.e. color intensity) compared to a known reference. The method is based on the Beer-Lambert law which states that there is a linear relationship between the concentration and absorbance of a solution, which means that the concentration of a solution can be calculated by measuring its absorbance.

A Triglyceride Assay Kit from Abcam (Ab65336) was used to perform the colorimetric analysis in this project. This kit contained:

- Triglyceride Assay Buffer, 25 mL
- Triglyceride Probe, 200 µl
- Lipase, 1 vial
- Triglyceride Enzyme Mix, 1 vial
- 1 mM Triglyceride Standard, 300 µl

In order to create a standard curve that could be used to calculate the concentrations of triglycerides in each liver sample, a 0.2 mM Triglyceride Standard was prepared by diluting 100 µl of the 1 mM Triglyceride Standard with 400 µl of Triglyceride Assay Buffer. 6 standard curve dilutions were then made by mixing together the newly prepared 0.2 mM Triglyceride Standard and Triglyceride Assay Buffer in different ratios (Table 2.1) and pipetting 50 µl of each mixture into a microplate to create the standard wells. Duplicates were made.

Table 1 Standard curve setup. Standard dilutions are used for creating a standard curve that can be used to calculate the concentration of triglycerides in a sample well.

Standard#	0.2 mM Triglyceride Standard (µl)	Triglyceride Assay Buffer (µl)	Volume used in standard well (µl)	Final amount of TG standard (nmol/well)
A	0	150	50	0
B	30	120	50	2
C	60	90	50	4
D	90	60	50	6
E	120	30	50	8
F	150	0	50	10

2.3.2 Sample and Control Wells

To create the sample wells, 23 frozen liver biopsies were thawed at room temperature and 50 mg of tissue were collected from each liver. Each sample was washed in cold PBS and suspended in 500 µl of 5% NP-40, a non-ionic detergent used to lyse plasma membranes, solubilize triglycerides, and prevent protein aggregation. The solutions were homogenized using a Dounce homogenizer for 15 passes before being tapped into a cuvette. All cuvettes were then put on a heating block at 95 °C for 3 minutes until the solutions became cloudy and were then cooled down to room temperature. Each cuvette was centrifuged at 13500 RPM and diluted 10-fold with 5 mL ddH_2O.

20 µl was then pippeted from each cuvette and added to the microplate in duplicates. 2 µl of lipase was added to all standard and sample wells, and 2 µl of Triglyceride Assay Buffer was added to sample background control wells (no lipase was added to the background controls). The microplate was then put on a microplate agitator at room temperature and mixed for 20 minutes to facilitate the breakdown of triglycerides into free glycerols and fatty acids. All plates were filled to a total volume of 50 ul by adding another 30 µl of triglyceride assay buffer.

2.3.3 Microplate Reading and Standard Curve

Finally, a 50 µl Triglyceride Reaction Mix was added to each well on the microplate. This mix consisted of 46 µl Triglyceride Assay Buffer, 2 µl Triglyceride Probe, and 2 µl Triglyceride Enzyme Mix. The microplate was then incubated in darkness at room temperature for 60 minutes and was then analysed by a microplate reader set to optical density (OD) 570 nm.

2.4 Reverse Transcription Quantitative PCR

The original central dogma of molecular biology, as stated by dr. Francis Crick in 1957, is that "once information has got into a protein it can't get out again". An alternative version of the central dogma that is commonly recited today, is that genetic information only flows in one direction, from DNA to RNA, and from RNA to protein (92). While the original central dogma still stands, the alternative version has been proven incorrect by the discovery of reverse transcriptase, which makes it possible for genetic information to flow from RNA back to DNA.

Reverse transcription quantitative polymerase chain reaction (RT-qPCR) is a molecular biology technique used to quantify gene expression levels in a sample by first reverse transcribing mRNA to complementary DNA (cDNA), and then amplifying the cDNA through PCR.

Simultaneously, a fluorescence dye (SYBR Green) is used to quantify the concentration of PCR-product by measuring fluorescence intensity. Fluorescence intensity is measured after each cycle of PCR and the number of cycles required before the fluorescence signal is stronger than background levels is referred to as the cycle threshold (Ct), or cycle of quantification (Cq) in Applied Biosystems instruments and software (Figure 8).

A lower Cq value indicates a higher amount of nucleic acid in the sample due to more RNA being made. A relative quantification is performed by normalizing the Cq values of the target genes to one or more reference genes – i.e. genes whose expression is not affected by the study conditions. In this project, a qPCR Analysis Excel-file made by lab engineers at the IMB laboratory was used to perform relative quantification of gene expression.

The Cq values from the reference genes *Hmbs* and *Cyclo* were used to calculate a geometric mean against which the test genes Cq values could be normalized. This resulted in a unitless ratio of relative gene expression.

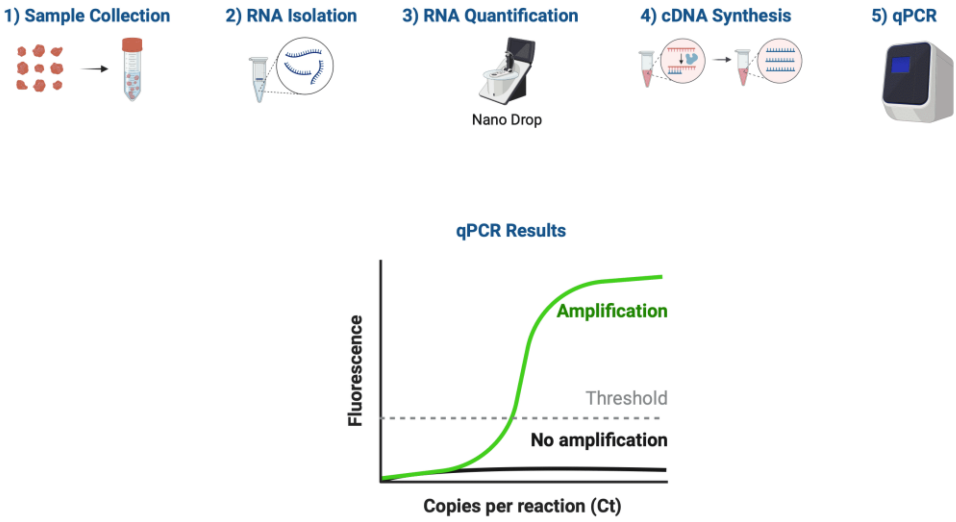

Figure 10 Graphic illustration of cDNA synthesis and qPCR. Sample tissue has to be dissolved so that the RNA can be isolated. RNA concentration is quantified using a NanoDrop machine. cDNA is then synthesized from the RNA and qPCR is performed. The result from qPCR is a Cq/Ct value, with a lower value indicating that there is more PCR product.

2.4.1 Sample Collection and RNA Isolation

RNeasy Plus Mini Kit and Buffer RLT Plus (QIAGEN) were used to purify RNA from the rat livers. These contained:

- RNeasy Mini Spin Columns, 50 pcs
- Collection Tubes (1.5 ml), 50 pcs
- Collection Tubes (2 ml), 50 pcs
- QIAzol Lysis Reagent, 50 ml
- gDNA Eleminator Solution, 8 ml
- Buffer RWT (concentrate), 15 ml
- Buffer RPE (concentrate), 11 ml
- RNase-Free Water, 10 ml
- Buffer RLT Plus, 220 ml

Before starting, 10 µl of β-Mercaptoethanol per 1 ml of Buffer RLT Plus were mixed togheter for a total of 10 ml lysis buffer. A Buffer RPE working solution had also been made by diluting 11 µl of the Buffer RPE concentrate with 44 µl 96% ethanol.

30 mg of tissue sample was then collected from 24 different liver biopsies and put in a 1.5 ml collection tube. 350 µl of the Buffer RLT Plus lysis buffer along with one stainless steel bead was added to each collection tube. The TissueLyser LT (QIAGEN) was then used to disrupt the tissue samples. The TissueLyser was set to 50 oscillations per minute for 2.5 minutes.

The homogenized lysate from each collection tube was then transferred to gDNA Eliminator Spin Columns placed in 2 ml collection tubes and centrifuged for 30 seconds at 13500 RPM. The gDNA columns were discarded after the centrifugation while the lysate flowthrough was saved. 350 µl lysate was then mixed with 350 µl of 70% ethanol by pipetting, and 700 µl of this mixture was transferred to RNeasy Mini spin columns that were placed in 2 ml collection tubes and centrifuged for 15 seconds at 13500 RPM.

The flowthrough from this centrifugation was discarded and the RNeasy mini columns were placed back into the collection tubes. 700 µl of Buffer RW1 was added to the RNeasy mini columns before centrifuging them again at 13500 RPM for 15 seconds and discarding the flowthrough. 500 µl of the Buffer RPE was then added to the RNeasy mini columns and centrifuged at 13500 RPM for 15 seconds.

The flowthrough was discarded and 500 µl Buffer RPE was added again and centrifuged at 13500 RPM for 1 minute. This flowthrough was also discared.

Finally, the RNeasy mini columns were moved to 1.5 ml eppendorf tubes, 50 µl RNase-free water was added, and the tubes were centrifuged at 13500 RPM for 1 minute. The RNeasy mini columns were then discarded and the Eppendorf tubes containing the flowthrough with isolated RNA was stored in a refrigerator.

2.4.2 RNA Quantification and cDNA Synthesis

In order to perform the cDNA synthesis, the High Capacity cDNA Reverse Transcription Kit from Applied Biosystems was used to reverse transcribe the isolated RNA samples. One drop from each RNA sample tube was analysed by using the NanoDrop 2000 Spectrophotometer from Thermo Scientific, and this concentration was used to calculate how many µl of RNA sample and ddH_2O should be mixed to achieve 1000 ng/µl (as recommended by the kit). To calculate this, we divided 1000 by the measured RNA concentration and then subtracted with number from 10. The new RNA tubes were stored on ice.

Table 2 Measured RNA concentration. The total volume for each cDNA tube was 10 µl. Fr = Fructose, Cr = Control.

Sample Code	Measured RNA conc (ng/µl)	µl of RNA sample	µl ddH_2O
A1-L-Fr	255.2	3.92	6.08
A2-L-Fr	142.1	7.04	2.96
B1-L-Cr	772.2	1.29	8.71
B2-L-Cr	311.5	3.21	6.79
C1-L-Fr	334.0	2.99	7.01
C2-L-Fr	20.2	10	
D1-L-Cr	350.2	2.85	7.15
D2-L-Cr	535.5	1.87	8.13
E2-L-Cr	620.2	1.61	8.39
F1-L-Fr	683.2	1.46	8.54
F2-L-Fr	261.5	3.82	6.18
G1-L-Cr	65.7	10	
G2-L-Cr	340.3	2.94	7.06
H2-L-Cr	239.2	4.18	5.82
I1-L-Fr	333.7	2.99	7.01
I2-L-Fr	538.3	1.86	8.14
J1-L-Fr	366.2	2.73	7.27
J2-L-Fr	144.7	6.91	3.09
K1-L-Cr	87.8	10	
K2-L-Cr	177.1	5.65	4.35
L1-L-Fr	445.2	2.25	7.75
L2-L-Fr	272.9	3.66	6.34

A cDNA Plus Mix containing the ingredients necessary for cDNA synthesis was then made, along with a cDNA Minus Mix containing the same ingredients except reverse transcriptase (Table 2.3). The purpose of the minus mix is to work as a control, indicating the reliability of the cDNA synthesis.

10 µl of the cDNA Minus Mix was added to four random RNA sample tubes and stirred by using a vortex mixer (IKA MS3 Basic). 10 µl of the cDNA Plus Mix was added to all other RNA samples and vortex mixed. All samples were incubated for 10 minutes at 25 °C, 2 hours at 37 °C, and 5 minutes at 95 °C before being cooled down to room temperature. The tubes

were then centrifuged at 13500 for 30 seconds before adding 60 µl of ddH_2O to each tube. All cDNA tubes were then stored in a refrigerator.

Table 3 Plus and minus mix for cDNA synthesis. The minus mix was added to four random sample tubes, and the plus mix was added to all remaining tubes. The minus mix did not contain reverse transcriptase.

RT Mix	**Per sample (µl)**
10 x RT Buffer	2
25 dNTP	0.8
10 x Random Primer	2
Reverse Transcriptase	1 (0 for the minus mix)
H_2O	4.2

2.4.3 Quantitative PCR

The quantitative PCR was performed by using the FastStart SYBR Green Master Kit from Roche (Hoffman-La Roche Ltd, Switzerland). A master mix and a series of diluted cDNA eppendorf tubes were made for each gene. The diluted cDNA series was made by first adding 20 µl of RNAse free H_2O to 4 eppendorf tubes and then adding 5 µl of sample from the previous dilution (Table 2.4). The master mix was made by mixing SYBR Green, forward and reverse primers, and RNAse free water in an eppendorf tube (Table 2.5).

Table 4 cDNA dilution series. Four dilutions were made for each gene to be used for measuring the qPCR efficiency. Efficiency in qPCR is a measure of how much DNA or RNA is amplified in each cycle.

Dilution	cDNA concentration
Tube 1) 20 µl H_2O + 5 µl cDNA	100%
Tube 3) 20 µl H_2O + 5 µl from tube 1	20%
Tube 3) 20 µl H_2O + 5 µl from tube 2	4%
Tube 4) 20 µl H_2O + 5 µl from tube 3	0.8%

Table 5 Master mix composition. A master mix contains the forward and reverse primers for the gene of interest, along with SYBR green which is the fluorescence dye used to quantify the amount of DNA or RNA made during each PCR cycle.

	Primer conc (200 nM)	**Primer conc (400 nM)**	**Primer conc (800 nM)**
SYBR Green	5 µl	5 µl	5 µl
Forward Primer	0.2 µl	0.4 µl	0.8 µl
Reverse Primer	0.2 µl	0.4 µl	0.8 µl
H_2O	2.6 µl	2.2 µl	1.4 µl

Five well-established reference genes from the IMB lab were tested as potential reference genes for this project, and the forward and reverse primer concentrations were 400/400 for each of these genes (Table 6). After qPCR had been performed, the software RefFinder was used to identify which genes were most stable and therefore best suited as reference genes (93). These were the HMBS and CYCLO genes (Appendix D).

Next up, 12 different genes available at the IMB laboratory were chosen as test genes on the basis of their role in the pathophysiology of MAFLD These were genes related to fatty acid metabolism, cellular stress, inflammation, fibrosis, and inter-organ crosstalk (Table 7).

This is a brief overview of all genes, with their proteins in parentheses. The proteins and their mechanisms are explained in greater detailed in sections 1.3.3 and 1.3.4.

Fatty acid metabolism

- Gene name: *Ppara* (peroxisome proliferator-activated receptor agonist alpha)
- Gene name: *Pparg* (peroxisome proliferator-activated receptor agonist gamma)
- Gene name: *Ppargc1a* (peroxisome proliferator-activated receptor gamma coactivator 1-alpha)
- Gene name: *Cpt1* (carnitine palmitoyl transferase-1)
- Gene name: *Pdk4* (pyruvate dehydrogenase kinase-4)

Cellular stress

- Gene name: *Ddit3* (C/EBP homologous protein, also known as CHOP)
- Gene name: *Atf4* (activating transcription factor 4)

Inflammation

- Gene name: *Il6* (interleukin-6)
- Gene name: *Tnfa* (tumor necrosis factor alpha)

Fibrosis

- Gene name: *Col1a1* (collagen, type I, alpha 1)
- Gene name: *Col3a1* (collagen, type III, alpha 1)

Inter-organ crosstalk

- Gene name: *Fgf21* (fibroblast growth factor-21)

Table 6 List of reference genes. Reference genes are genes whose expression levels remain stable under the study conditions. Five different reference genes available at the IMB laboratory were tested.

Gene	Accession number	Sequence (5'-3')	Primer concentration
Cyclo	NM_017101.1	RP:CTGATGGCGAGCCCTTG FP:TCTGCTGTCTTTGGAACTTTGTC	400/400
Gapdh	NM_017008.3	FP:TGGGAAGCTGGTCATCAAC RP:GCATCACCCCATTTGATGTT	400/400
Hprt1	NM_012583.2	FP:GACCGGTTCTGTCATGTCG RP:ACCTGGTTCATCATCACTAATCAC	400/400
Sdha	NM_130428.1	FPCCCTGAGCATTGCAGAATC RP:CATTTGCCTTAATCGGAGGA	400/400
Hmbs	NM_013168.2	FP:TCTCTGAAGGATGTGCCTAC RP:ACAAGGGTTTTCCCGTTTG	400/400

Table 7 List of test genes. Twelve different test genes chosen for this project. Choice of test genes were based on NAFLD pathophysiology and available optimized primers at the IMB laboratory.

Gene	Accession number	Sequence (5'-3')	Primer concentration
Col1a1	NM_053304.1	FP:CATGTTCAGCTTTGTGGACCT RP:GCAGCTGACTTCAGGGATGT	400/400
Col3a1	NM_032085.1	FP:TCCCCTGGAATCTGTGAATC RP:TGAGTCGAATTGGGGAGAAT	400/400
Pparg	NM_013124.3	FP:CACAATGCCATCAGGTTTGG RP:GCTGGTCGATATCACTGGAGATC	400/400
Ppara	XM_039078501.2	ACGATGCTGTCCTCCTTGA GTGTGATGAAGCCATTGCC	400/400
Pdk4	NM_053551.1	FP:GCATTTCTACTCGGATGCTCATG RP:CCAATGTGGCTTGGGTTTCC	400/400
Cpt1	XM_063282351.1	FP:GCACCAAGATCTGGATGGCTATGG RP:TACCTGCTCACAGTATCTTTGAC	400/400
Ppargc1a	NM_031347.1	FP:GTGCAGCCAAGACTCTGTATGG RP:GTCTGTGTCCAGGTCATTCACA	200/200
Fgf21	NM_019113.4	FP:GGGTCAAGTCCGACAGAGGTAT RP:ATCAAAGTGAGGCGATCCATAGA	400/400
Ddit3	XM.006241444.4	FP:GCGACAGAGCCAGAATAACA RPGATGCACTTCCTTCTGGAAC	400/400
Atf4	XM_039079942.1	FP:CTCTTCTTCTGGCGGTACCT RP:CTCTTCTTCTGGCGGTACCT	400/400
Il6	NM_012589.2	FP:AGAGACTTCCAGCCAGTTGC RP:AGTCTCCTCTCCGGACTTGT	400/400
Tnfa	NM_012675.3	FP:GCCCAGACCCTCACACTC RP:CCACTCCAGCTGCTCCTCT	200/200

2.5 Statistics and Software

Data collection was performed using Microsoft Excel version 16.83 for Mac. Statistical analysis was conducted using RStudio version 2023.12.0.369 and the Tidyverse package. The threshold for accepting statistical significance was established as $p<0.05$ for all tests. Digital image analysis was performed by using QuPath v 0.4.4. Images are either made or premade in BioRender. The frontpage image was made using ChatGPT 4.0.

The variables body weight (BW), liver weight (LW), fat mass (FM), triglycerides (TG), Oil Red O stain (ORO), Picro Sirius Red stain (PSR), and systolic blood pressure (SBP) were imported to RStudio. All variables were checked for normality with the Shapiro-Wilk test. BW, LW, TG and SBP were normally distributed and Levene's test for Homogeneity of Variance was performed. Testing for normality and heteroscedasticity is important for knowing which type of statistical tests to use in order to avoid reducing the power of the tests, which is the ability of the test to correctly identify a difference between the groups being compared.

With the assumptions of normality and heteroscedasticity being tested and confirmed, a two tailed independent samples t-test (parametric test) was performed on BW, LW, TG and SBP. Wilcoxon rank sum test (non-parametric test) was performed on FM, ORO and PSR. Parametric data is presented in tables or bar graphs as mean±SD, while non-parametric data is presented using box plots. Exceptions are made for FM and LW which are presented in table 8 along with the other characteristics as mean±SD for uniformity, and because they were significant in both parametric and non-parametric tests, and the means and medians are close. SD is chosen to present variability around the mean instead of SE, because SE should be limited to inferential statistics as it is technically a SD of multiple means (94).

For H&E staining, a Fischer's exact test was performed to test for a difference in macrovesicular and microvesicular steatosis between the fructose group and control group.

For qPCR, results are presented similarly as in the qPCR analysis file from the IMB laboratory, which is bar charts with mean±SE. An asterix have been added above significant results from two-sample independent t-tests.

3 Results

3.1 Characteristics

Body weight, liver weight, fat mass, and systolic blood pressure were measured by laboratory staff prior to the beginning of this master's project, but these characteristics will be presented here due to their importance in interpreting the results. At baseline, there was no significant difference in body weight or systolic blood pressure between the fructose and control group. At week 16 there was a significant difference in body weight, systolic blood pressure, liver weight, and fat mass.

Table 8 Group characteristics. Characteristics of the fructose and control group at baseline and week 16. Data presented as mean±SD

	Control (n = 12)	**Fructose (n = 12)**	**Significant (p<0.05)**
Body weight (baseline)	535±20 g	545±17 g	No ($p=0.24$)
Body weight (wk 16)	658±26 g	736±36 g	Yes ($p=3.5x10^{-6}$)
% change from baseline	22.99%	35.05%	
Systolic blood pressure (baseline)	135±13 mmHg	131±13 mmHg	No ($p=0.56$)
Systolic blood pressure (wk 16)	120±15 mmHg	135±11 mmHg	Yes ($p=1.1x10^{-2}$)
% change from baseline	-11.11%	3.05%	
Liver weight (wk 16)	19±1 g	26±2 g	Yes ($p=1.4x10^{-10}$)
Fat mass (wk 16)	19±10 g	59±28 g	Yes ($p=1.0x10^{-4}$)

3.2 Liver Histology

3.2.1 Hematoxylin and Eosin Staining Results

There was a significant difference in the presence of microvesicular steatosis ($p=2.5x10^{-5}$) and macrovesicular steatosis ($p=1.4x10^{-3}$) between the fructose and control group, but no hepatocellular hypertrophy or inflammatory cells were found (Fig. 11, Table 9, Table 10).

Three areas of 250000 μm^2 per slide were divided into 10 smaller squares of 2500 μm^2 using QuPath, and each square was visually inspected with the help of reference images from Liang et al (2014) (91). The difference between macrovesicular and microvesicular steatosis according to this paper is that the nucleus is displaced in macrovesicular steatosis, making the cell appear as a white, empty circle. Hypertrophy is defined as a cellular enlargement more than 1.5 times the normal hepatocyte diameter, and inflammation is evaluated by counting the number of inflammatory cells per focus square.

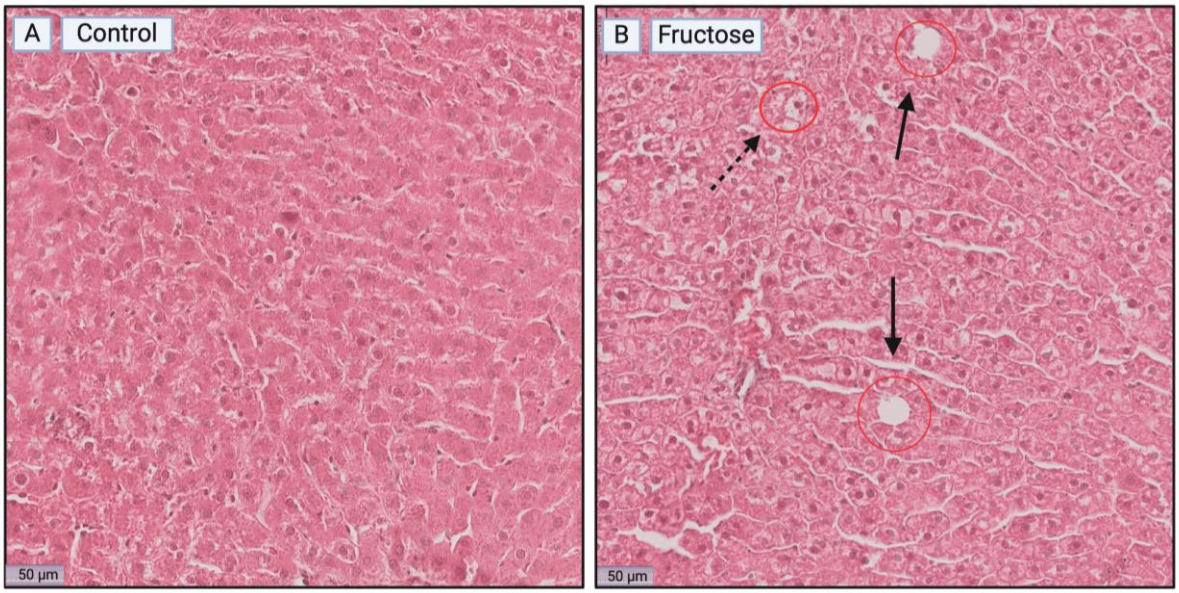

Figure 11 Examples of macrovesicular and microvesicular steatosis shown by H&E staining. Dashed arrow indicates microvesicular steatosis and normal arrow indicates macrovesicular steatosis. No hepatocellular hypertrophy or inflammatory cells, as illustrated by reference images in the paper by Liang (91), were found.

Table 9 Results of Fisher's exact test. The null hypothesis is that there is no association between two categorical variables (fructose and steatosis) and is appropriate when the sample size is small.

	Macrovesicular steatosis	No steatosis	Total	
Fructose	6	3	9	**p-value**
Control	2	8	10	1.4×10^{-3}
Total	8	11	38	
	Microvesicular steatosis	**No steatosis**	**Total**	
Fructose	9	0	9	**p-value**
Control	5	5	10	2.5×10^{-5}
Total	14	5	38	

Table 10 NAFLD inspection table. Reference images from a general NAFLD scoring system for rodent models were used to identify the presence of macro- and microvesicular steatosis, hepatocellular hypertrophy, and inflammation. F = fructose, C = control.

	Macrovesicular steatosis		Microvasicular steatosis		Hepatocellular hypertrophy		Inflammation	
Sample (N = 19)	**yes**	**no**	**yes**	**no**	**yes**	**no**	**yes**	**no**
A2-F	x		x			x		x
C1-F	x		x			x		x
C2-F		x	x			x		x
F1-F	x		x			x		x
F2-F		x	x			x		x
I1-F	x		x			x		x
I2-F	x		x			x		x
J1-F		x	x			x		x
J2-F	x		x			x		x
D1-C		x		x		x		x
D2-C		x		x		x		x
E1-C	x		x			x		x
E2-C		x	x			x		x
G1-C		x	x			x		x
G2-C		x	x			x		x
H1-C	x		x			x		x
H2-C		x		x		x		x
K1-C		x		x		x		x
K2-C		x		x		x		x

3.2.2 Picro Sirius Red Staining Results

There was no significant difference in the median amount of picro sirius red stain per slide (1.40% for the fructose group, 2.98% for the control group, p=0.55) suggesting that fructose-treatment did not lead to increased collagen deposition in the liver (Fig. 12).

Three areas of 250000 μm^2 per slide were randomly chosen and the amount of stain was quantified. The average amount of stain in each slide was used as the final measurement for each slide.

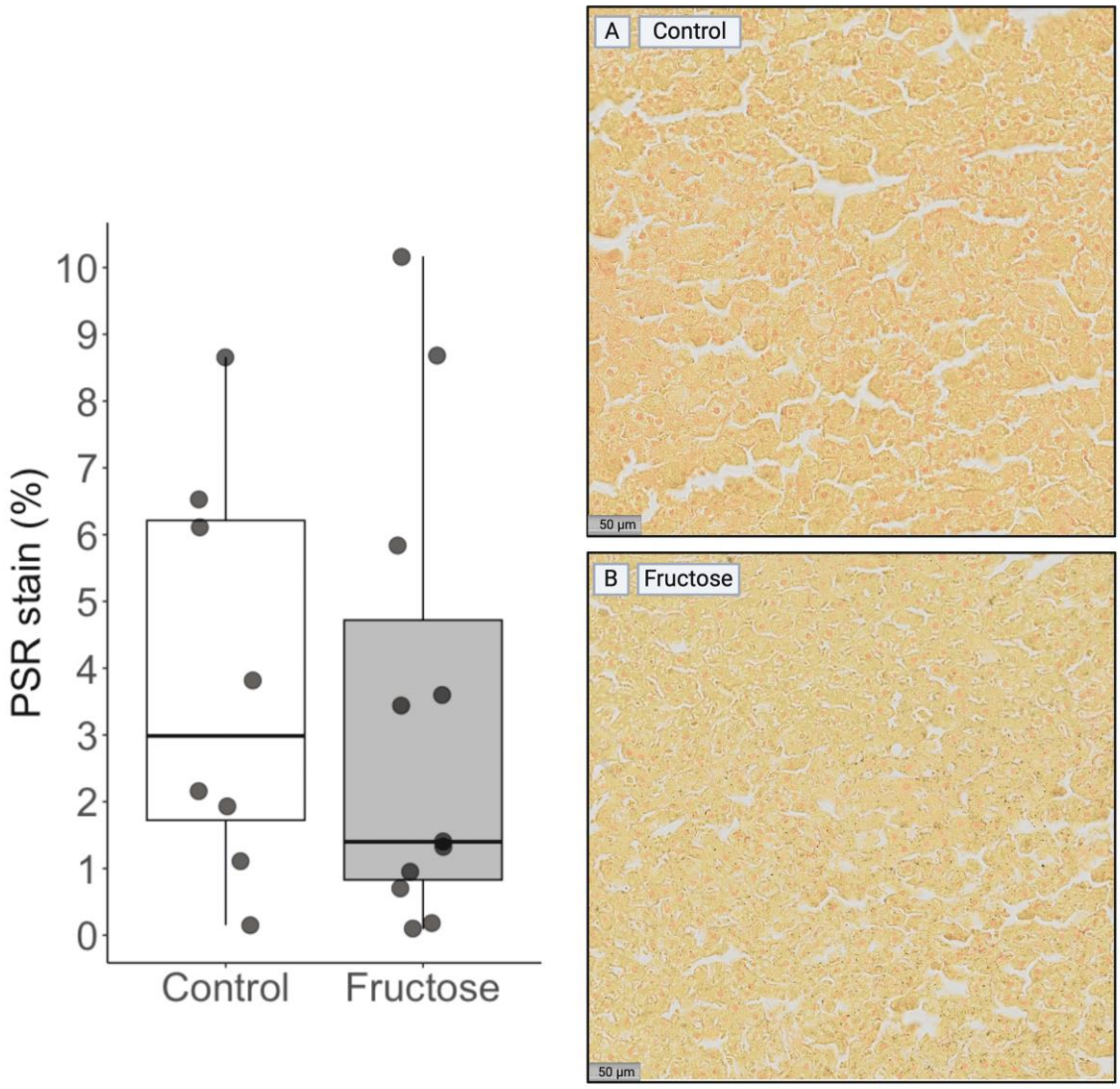

Figure 12 Box plots and sample images of PSR staining. Boxes represent median±IQR, Whiskers represent Q1-1.5*IQR (lower) and Q3+1.5*IQR (upper) with outliers outside. n = 19. Statistical test (wilcoxon rank sum) *p<0.05. Fructose vs control.

3.2.3 Oil Red O Staining Results

There was a significant difference in the median amount of ORO staining (2.78% for the fructose group, 0.06% for the control group, $p=4.94x10^{-4}$) suggesting that fructose-treatment led to increased lipid deposition in the liver (Fig. 13). The same procedure as in PSR staining was used: Three areas of 250000 μm^2 per slide were randomly chosen and the amount of stain in each area was quantified, and the average amount of stain in each slide was used as the final measurement for each slide.

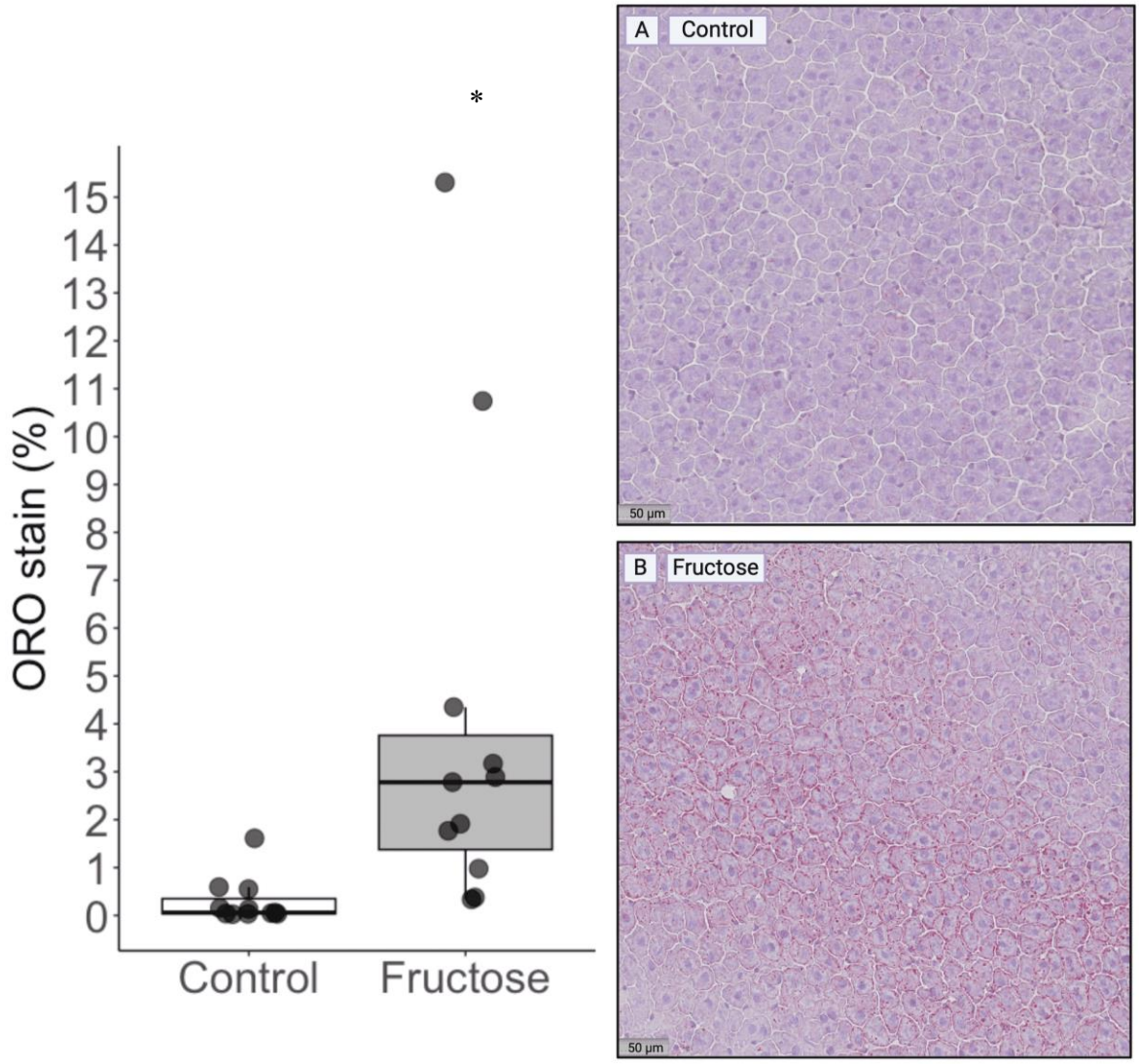

Figure 13 Box plots and sample images of ORO staining. Boxes represent median±IQR, Whiskers represent Q1-1.5*IQR (lower) and Q3+1.5*IQR (upper) with outliers outside. n = 22. Statistical test (wilcoxon rank sum) *p<0.05. Fructose vs control.

3.3 Liver Triglyceride Content

There was a significant difference in mean triglyceride levels between the fructose and control group (1.79±0.67 nmol/µl in the fructose group, 1.16±0.39 nmol/µl in the control group, P=0.01178).

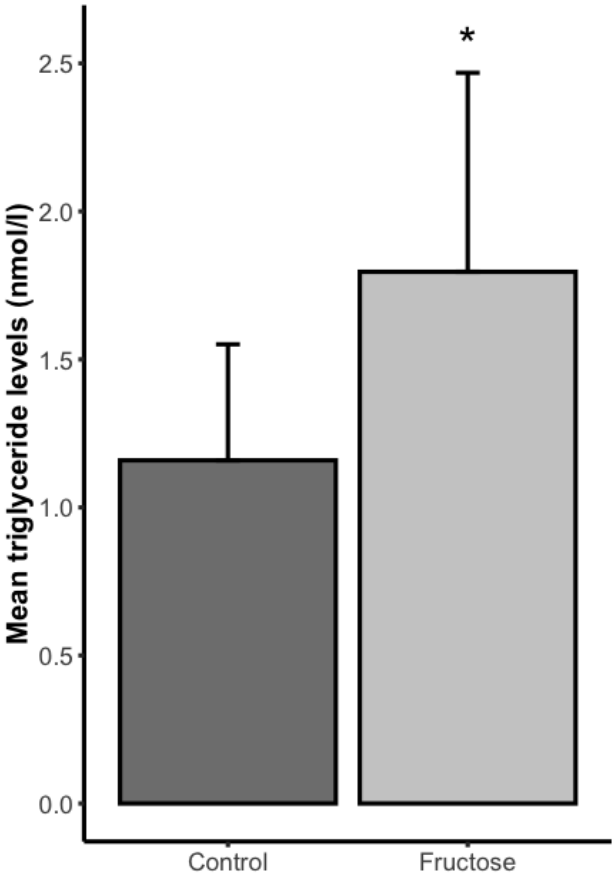

Figure 14 Bar graphs showing mean triglyceride levels. Data are mean±SD, n=23. *p<0.05. Fructose vs controls.

The results from the triglyceride assay were put into an Excel-file and a standard curve was made from the corrected absorbance of the standard wells (Table 11 and Figure 14). The corrected absorbance was calculated by subtracting the absorbance from standard well A where no triglyceride standard was added.

Table 11 Results of standard wells from microplate reader. The corrected absorbance of the standard wells was calculated by subtracting the absorbance of tube A, which had no triglyceride standard added, from the remaining tubes B–F. A standard curve was then made.

Tube	Concentration	Absorbance	Corrected Absorbance
A	0	0.054	0.000
B	2	0.083	0.0029
C	4	0.103	0.049
D	6	0.148	0.095
E	8	0.213	0.159
F	10	0.266	0.212

Figure 15 Standard curve. The standard curve is used for estimating the triglyceride concentration by rearranging the linear regression equation. 96% of the variance in absorbance (dependent variable) can be explained by the concentration (independent variable) as shown by $R^2 = 0.9632$.

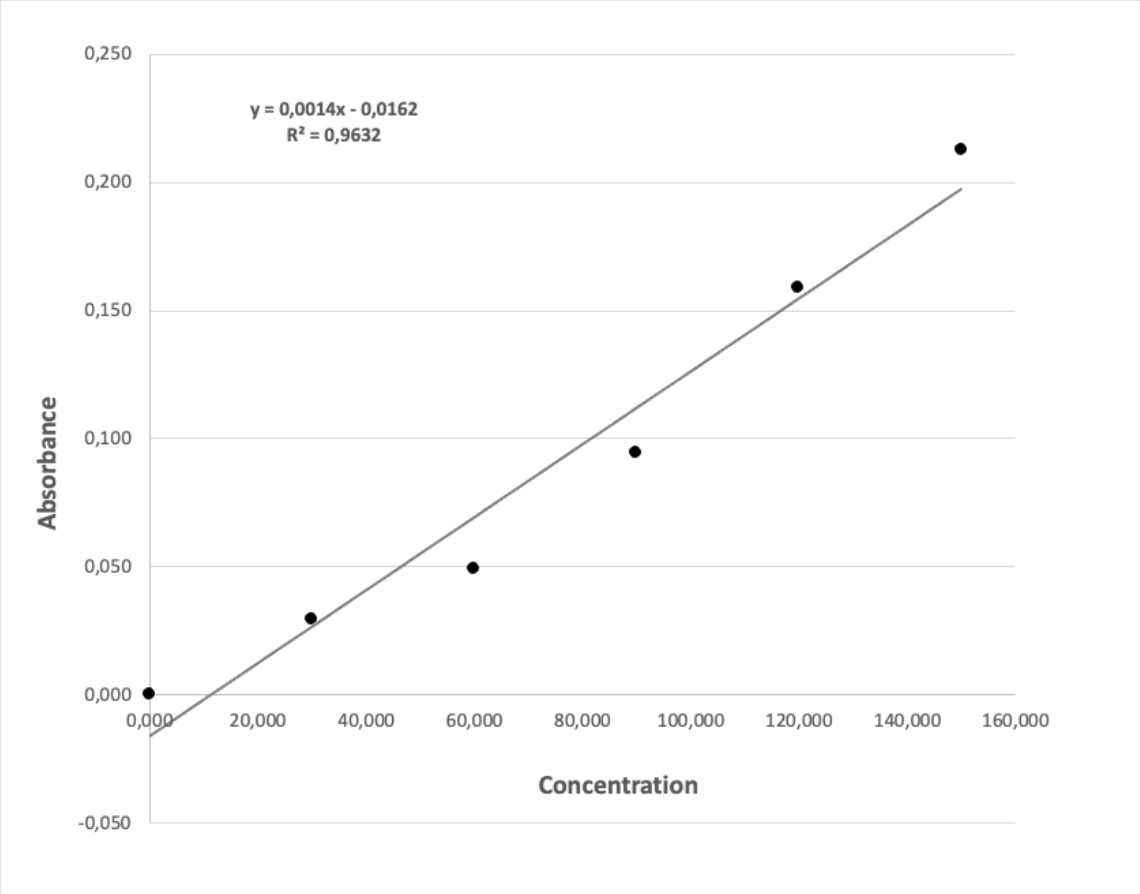

The standard curve is expressed as a linear regression line y = a+bx, where y is the predicted absorbance, x is the concentration, a is the intercept where the regression line crosses the y-axis, and b is the predicted change in y (absorbance) for every unit change in x (concentration). By rearranging the formula, we estimated x which is the concentration in nmol/well.

$$y = 0{,}0014x - 0{,}0162 \quad \Rightarrow \quad x = \frac{y + 0{,}162}{0{,}0014}$$

We can then calculate the concentration in nmol/µl by using this formula. Here, x is the amount of nmol/well, V is the sample volume added to each well, and D is the dilution factor.

$$\frac{\text{nmol}}{\text{ul}} = \left(\frac{x}{V}\right) * D$$

Table 12 Results of test wells from microplate reader. The concentration in nmol/µl was calculated by using the results from the standard wells to create a standard curve, and then rearranging its equation.

Tube	Concentration (nmol/well)	Average Absorbance	Corrected absorbance	Concentration (nmol/µl)
A1-F	216,000	0,340	0,286	1,08
A2-F	150,607	0,248	0,195	0,75
B1-C	125,143	0,213	0,159	0,63
B2-C	359,750	0,541	0,487	1,80
C1-F	334,929	0,506	0,453	1,67
C2-F	388,036	0,581	0,527	1,94
D1-C	264,714	0,408	0,354	1,32
D2-C	214,214	0,337	0,284	1,07
E2-C	153,071	0,252	0,198	0,77
F1-F	374,107	0,561	0,508	1,87
F2-F	366,571	0,551	0,497	1,83
G1-C	250,500	0,388	0,335	1,25
G2-C	226,000	0,354	0,300	1,13
H1-C	320,714	0,487	0,433	1,60
H2-C	133,571	0,225	0,171	0,67
I1-F	227,714	0,356	0,303	1,14
I2-F	593,714	0,869	0,815	2,97
J1-F	309,571	0,471	0,417	1,55
J2-F	452,286	0,671	0,617	2,26
K1-C	187,143	0,300	0,246	0,94
K2-C	313,857	0,477	0,423	1,57
L1-C	578,643	0,848	0,794	2,89
L2-C	319,357	0,485	0,431	1,60

3.4 Liver Gene Expression

Increased fat storage in the liver following fructose treatment was associated with altered cellular metabolism demonstrated by the marked decrease in the expression of the PPAR target gene *Pdk4* (p=0.0411) in the fructose-treated rats, although no significant changes in *Ppara* or *Ppary* expression were observed (Fig. 16). In livers from fructose-treated rats, there was also an upregulation of Atf4 related to cellular stress (p=0.0194), and an upregulation of FGF21, possibly related to inter-organ crosstalk (p=0.0213).

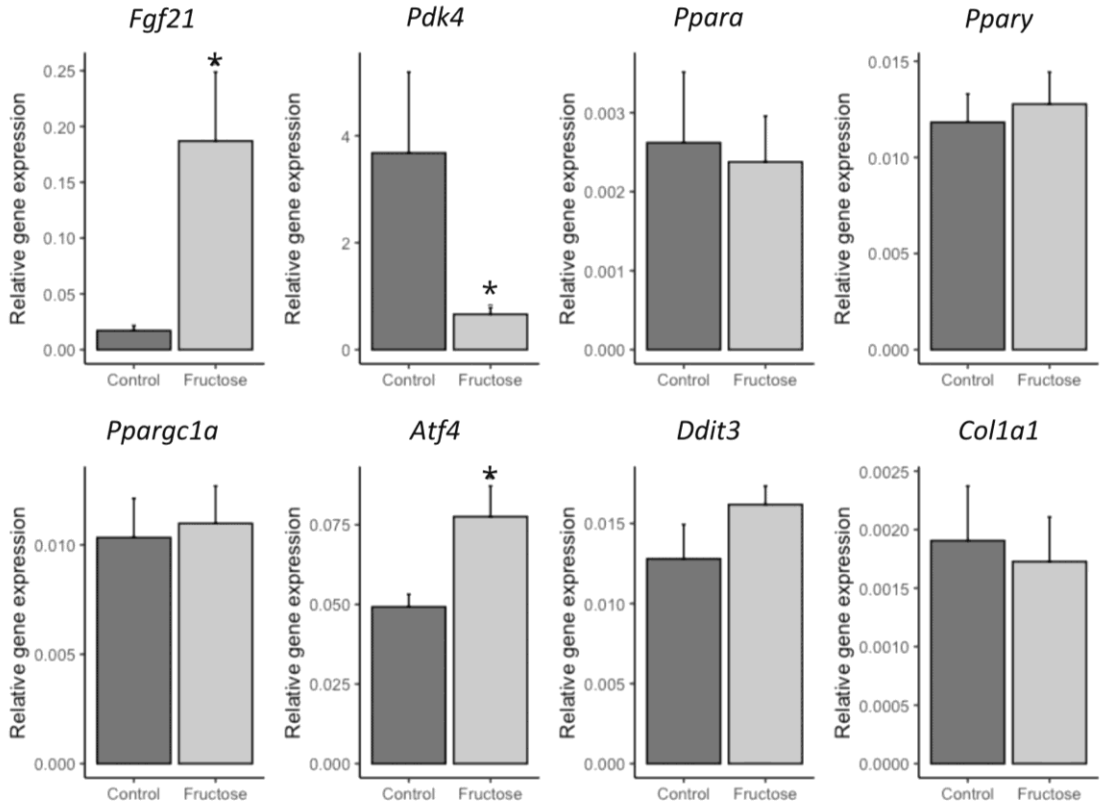

Figure 16 Relative expression of test genes. Data are mean±SD, n=22.
*p<0.05. Fructose vs controls. Genes involved in inter-organ crosstalk: *Fgf21*, Genes involved in fatty acid metabolism: *Ppara*, *Ppary*, *ppargc1a, Pdk4*. Genes involved in cellular stress: *Ddit3*, *Atf4*. Genes involved in fibrosis: *Col1a1*.

Relative quantification of gene expression was performed by using a qPCR Analysis Excel-file developed by staff at the IMB laboratory. The Cq values from the reference genes HMBS and CYCLO were used to calculate a geometric mean against which the test genes Cq values could be normalized. This resulted in a unitless ratio of relative gene expression. Due to

issues that could be related to primer optimization, only 8 of 12 genes could be quantified by qPCR. The genes that could not be quantified were *Cpt1*, *Il6*, *Tnfa*, and *Col3a1*.

4 Discussion

4.1 Main findings

16 weeks of high fructose feeding led to increased body weight, fat mass, liver weight, and blood pressure in male Sprague-Dawley rats. The histological analysis and triglyceride assay show that there was evidence of fatty liver without evidence of fibrosis or inflammation, and mRNA expression levels suggest altered liver metabolism in response to increased cellular stress.

These findings are in line with the systematic review and meta-analysis by Toop and Gentili showing that the chronic consumption of beverages containing 10-21% fructose is associated with increased body weight and markers of metabolic syndrome in rodents (85). There was also an increase in systolic blood pressure in the fructose group, and it has been shown in a study for Chen et al (2019) that 10% fructose feeding for just one week can lead to elevated blood pressure due to impaired baroreflex sensitivity and overactivity of the sympathetic nervous system (95).

It is also important to add that as the amount of hepatic steatosis in the current project was low in both groups, but the rats in the fructose group were arguably in a state of low-grade or early-stage NAFLD. This would also explain the small amount of collagen in both groups, as this is a marker of late-stage NAFLD (i.e. NASH and cirrhosis). There was also no difference in the expression of COL1A1 mRNA, which would be expected to be upregulated in the fructose group if there had been more collagen present (96,97).

Expression of *Fgf21* mRNA was increased in the fructose group, and a study from Dushay et al (2015) has shown that fructose ingestion increases circulating levels of FGF21 in humans (98). This response to fructose has also been shown to be present in rodents by Fisher et al (2019) (99). Seeing as FGF21 is mainly produced in the liver and is known to exert protective effects against hepatic steatosis by suppressing inflammation and fibrosis, increasing fatty acid oxidation, and decreasing de novo lipogenesis (100,101), the upregulated expression of

FGF21 mRNA seen in the fructose group may reflect an adaptive and compensatory response to the metabolic stress induced by the high fructose intervention.

Atf4 mRNA expression is activated during ER stress as part of the UPR response (83,84). The UPR response aims to restore cellular homeostasis by reducing protein translation and assisting in proper protein folding and trafficking, but also activates apoptosis pathways if homeostasis is not restored (102). It has been shown that *Atf4* deficiency protects against fructose-induced MAFLD in mice by reducing hepatic PPARγ, SREBP-1c, acetyl-CoA carboxylase, and fatty acid synthase expression (103).

Pdk4 mRNA expression and protein levels are elevated in the livers of diabetic, fasted and insulin resistant animals (104), but in this project the expression was decreased in the fructose group. This difference might be due to the low amount of hepatic steatosis in the fructose group. There might also be a relationship between *Fgf21* and *Pdk4*, as injection of FGF21 in obese mice has been shown to downregulate hepatic *Pdk4* expression (100).

4.2 Strengths and Limitations

4.2.1 Sectioning and Staining

There are many steps and procedures involved in the sectioning and staining of paraffin-embedded and OCT-embedded (frozen) tissue that can be challenging for an untrained operator, which was the case in this project, and this could have affected the interpretability of the results. Despite having an initial 24 blocks of sample tissue, some of the samples became slightly damaged, and some became unusable, during either the sectioning, staining or mounting phase.

The rotary microtome used to section the paraffin-embedded tissue was connected to a water slide that transferred sections to a lukewarm water-bath. During the sectioning process, the thickness setting of the microtome, temperature of the specimen holder, and the speed of the rotating blade can affect the quality of the samples.

After several sectioning attempts where the samples became completely folded, the automatic rotation of the cutting blade was turned off and all sections were manually cut at slow speed. The thickness of the paraffin-embedded sections was also increased to 5 µm from 3 µm, which is at the upper-end of the thickness used in other papers (105–107). These decisions

seemed to make the samples less folded, and when they rested in the water-bath they seemed to unfold completely. There is a possibility that the initial folding of the samples could have damaged some of the tissue architecture. However, the samples were visually inspected by a lab engineer and were considered to be of a sufficient quality.

The OCT-embedded tissue was sectioned in a cold environment and a room-tempered microscope slide was placed on top of each sample to attach them. During the attachment, some samples seemed to fold slightly which upon contact with the slides, which could affect image quality. The choice of 10 μm section thickness for OCT-embedded tissue were based on existing literature and discussion with a lab engineer (108). These samples were also inspected and considered to be of sufficient quality.

During the staining phase the slides were dipped in many jars of different solutions and some of them were rinsed with water from a pipette. It is possible that some slides could have been damaged during these staining procedures. The mounting mediums used for both paraffin-embedded samples (Histokitt) and OCT-embedded samples (Mowiol) was thick and viscous, and this could have also damaged the samples if the tissue was fragile.

During ORO staining, no red spots (lipid droplets) were found when using a normal light microscope after following standard procedure. A second attempt was made, where the samples were soaked in the Oil Red O solution overnight. At first glance in a light microscope this did not seem to have an effect, but when using a slide scanner we could see red spots. The first ORO stained samples had been discarded, so it is uncertain whether the problem is that the ORO kit was out of date, that the first light microscope was old and maybe in poor condition, or that the samples should have been soaked overnight from the beginning.

4.2.2 Digital Image Analysis

4.2.2.1 Analysis of Picro Sirius Red Staining and Oil Red O Staining

QuPath is a bioimage analysis software developed by dr. Peter Bankhead and colleagues at Queen's University Belfast (90). Though it was designed to be a user-friendly tool for digital image analysis, it was designed for clinical pathology. As the aim of the project was to investigate if there was a difference between the livers of the fructose and control group, it

was decided to choose a simple approach to quantify this difference rather than use more elaborate and technical approaches that a trained pathologist may have used.

PSR and ORO staining was quantified by comparing the amount of area stained in each sample. Identification of the stains had to be done manually in the beginning to teach the software to recognize the right colors, and a thresholder (color identification tool) was then made in QuPath to automate the process. However, some images had different color tones which means that separate thresholders had to be made for these images, and even then, the thresholders identified large amounts of stain compared to the other slides. This is apparent in the outlier data points seen in figure 3.2.3.1. Despite this, the significant (ORO) and non-significant (PSR) findings were still present when removing the outliers, and it was decided to keep all data and show each data point using box plots.

For PSR staining, only bright-field microscopy was used in the slidescanner, but we could also have used polarized light which could be used to discriminate between different types of collagen fibers (109,110).

4.2.2.2 Analysis of Hematoxylin and Eosin Staining

For H&E staining, we were unable to quantify the presence of NAFLD through any automated process such as identifying and discriminating between different types of steatosis. This may be due to the fact that all samples showed very little signs of NAFLD (Fig. 6). Thus, it was decided to quantify the difference by manually screening each sample and tabulating the results separately as seen in tables 3.2.1.2 and 3.2.1.3.

No positive or negative controls of NAFLD from rat livers were available in the lab, and therefore sample images from a paper by Liang et al (2014) were used to help identify NAFLD/NASH (91). This paper was chosen because it systematically compares and considers the differences between rodent and human liver pathology. Although liver biopsies are the gold standard for NAFLD/NASH diagnosis, this is an invasive procedure that is only done in high risk human subjects. This means that scoring systems made for humans are skewed towards more severe forms of NAFLD – the most common ones being the Brunt scoring system and the NASH-CRN/Kleiner scoring system (111,112).

It is possible that the tabulation might yield different results if performed by other investigators. However, a quick visual inspection was performed by two trained pathologists and neither one could identify any obvious signs of NAFLD.

4.2.3 Triglyceride Quantification

During the triglyceride assay there was a step where the cuvettes containing the sample tissue were heated to 95 °C for 3 minutes. At the end of the 3 minutes some of the cuvettes were so hot that the lids popped open, and it is possible that some of the contents from the cuvettes was lost. These cuvettes were quickly placed on ice and cooled down. As it seemed to only be foam that was lost from the cuvettes, we continued following the procedure. Only 3 or 4 cuvettes lost foam but this may have contributed to variation in the results.

4.2.4 RT-qPCR

During the RT-qPCR, two wells were made for all samples. However, although RT-qPCR was performed on 12 different genes (in addition to housekeeping genes), only 8 of these genes could be quantified. This was probably related to primer optimization, because 2 more attempts were made for each of these genes with no success.

4.2.5 Strengths

The strength of this project is that three different histological techniques, a biochemical analysis (triglyceride assay), and gene expression analysis (qPCR) all converge to show that there was indeed more fat accumulation in the livers of the fructose group compared to the control group. Convergence of many lines of evidence strengthen the conclusion that the high fructose feeding led to a state of early-stage MAFLD.

4.3 Other Considerations

4.3.1 The importance of basic research

The purpose of basic research is to understand the mechanisms that link together a cause and effect at the molecular level. However, translating results from basic science to clinical practice, also referred to as translational medicine, has proven to be a major challenge (113). However, when it does succeed, it can have a profound impact on both clinical practice and public health policy. For example, the quick development of the covid-19 mRNA vaccines was built on a bedrock of basic research that had been years in the making, starting with the discovery of mRNA in the 1960s (114).

The high prevalence of MAFLD has serious consequences, not only in increasing the number of people requiring liver transplants, but also in decreasing the number of healthy livers available for donation (115). There is currently no effective pharmaceutical intervention for MAFLD, and the only effective intervention is lifestyle change. Pharmacological and lifestyle interventions are not mutually exclusive but rather complementary to each other depending on a number of factors such as disease stage, co-morbidity, personal and financial resources.

4.3.2 Of Rats and Men

Approximately 90% of the Nobel Prizes in Physiology or Medicine have been related to animal research, highlighting the importance of animal experiments to improve understanding of human physiology in health and disease (116). Almost 80% of the animals used for experimental purposes are rodents, and 20% of these rodents are rats (117). While all mammalian cells use similar molecular mechanisms to regulate metabolism (including growth, replication, differentiation and cell death) (118), there are also many important factors to consider when interpreting data from rats and other rodents such as mice.

Humans are about 300 times larger than rats and 3000 times larger than mice, measured in kilograms (119). Rats age almost 27 times faster than humans and live up 3 years, compared to 80 years on average for humans, and have a 6.4 times faster basal metabolic rate (120). Across their entire life span, 14 rat days can generally be considered equivalent to 1 human year but this is also depends on their developmental stage (121). Reaching adulthood takes approximately 210 rat days or 7 months, and in adulthood 12 rat days are equivalent to 1 human year (120,121).

In this project, the Sprague-Dawley rats were aged 10–12 weeks on arrival and the intervention lasted for 16 weeks. Translated to human physiology, this is similar to putting young adults on an ad-libitum high fructose intervention for approximately 7-8 years. It is important to remember that the main purpose of this intervention was study mechanisms, and therefore it is not expected that the intervention should necessarily mimic reasonable human conditions, although the standard western diet reasonably can be considered a type of high-fructose intervention as well (122).

Temperature and circadian rhythm can also affect metabolism. The thermoneutral zone is the temperature range where an organism doesn't expend energy to maintain its internal temperature, and is approximately 26–36 °C for animal mice and rats (123,124). The housing temperature used in this project was 21 °C which is slightly below the lower threshold and can induce a cold stress response which affects metabolism cardiovascular parameters, respiration and immunity (125). Tests related to memory and cognitive functions were also performed in the rats during the 16-week intervention period, and these were performed during regular work hours which is the resting hour of rats. This disruption of circadian rhythm can also affect metabolism and increase expression of genes related to fat storage (126).

Another important consideration is that this project only looked at male Sprague-Dawley rats, which may affect generalization of the findings (127). Exhaustive exercise has been shown to elicit different responses in male and female rats, with glucose-, fatty acid-, and amino acid metabolism and TCA cycling increasing in males, whereas females utilize more lipids and conserve carbohydrate and proteins to a higher degree (128). It is a possibility that this sex difference also is present in less strenuous situations as well. Future investigations will include female reats in order to study potential

A final important distinction between humans and rodents is that rodents have the enzyme uricase which humans lack. This means that rats are less susceptible to hyperuricemia and gout, and it has been shown that male uricase-deficient rats (which are not used in this project) are better suited as models for studying hyperuricemia and associated diseases in humans (129) which may be relevant for studying the effects of chronic high fructose intake.

4.3.3 Statistical Significance and Clinical Significance

There are two main philosophical branches within the world of statistical analysis: Bayesian statistics and Frequentist statistics (130). Conceptually, the main difference is that Bayesian statistics take prior information into consideration by ascribing probability distributions to population means and proportions, whereas Frequentist statistics assume that population values are fixed (130).

The majority of academia works within the framework of Frequentist thinking, which has made the concept of null hypothesis significance testing (NHST) a cornerstone in modern scientific practice. In NHST, we first make an assumption that there is no difference between the data being compared (the null hypothesis), and an alternative hypothesis (the test hypothesis) is tested against this null assumption (131).

The p-value is an estimate of the chances of getting a test result that is at least as extreme as the one observed, assuming that the null hypothesis and all of its assumptions are true, and has traditionally been set at a threshold of 0.05 (132). If $p < 0.05$ we call it statistically significant and declare that we 'reject the null hypothesis', or we declare that we 'fail to reject the null hypothesis' if $p > 0.05$. However, a statistically significant effect is not necessarily clinically important (133).

Prospective human outcome data are the strongest levels of evidence for influencing clinical guidelines and public health policies, but due to practical and ethical reasons, interventional trials with hazardous exposures can not be done on human subjects whereas animal models allow us to do many experiments that would otherwise be impossible to get done (134,135). The ability to tightly control the exposure and experimental conditions of animal models and cell lines also increases the researcher's confidence in the strength of causality. However, the artificial conditions of the experiment could also mean that the results will not hold true under more dynamic conditions where biochemical reactions are influenced by a number of other factors (113,123,135).

With this context in mind, the results from this study show that there is a difference between the fructose and control group, and due to the randomisation process it is fair to assume that all known and unknown confounding variables are considered (136). The result from this project warrants further investigation.

4.3.4 Future perspectives

Originally, we also wanted to investigate cardiac tissue, brain tissue, and blood samples to see if expression of FGF21, FGF21-receptor and its co-receptor β-klotho was increased. This would have provided valuable insights into the main aims of the larger translational study which this project is a part of, which is to investigate if FGF21 is a mediator of inter-organ crosstalk between the liver, heart, and brain. Due to time and resource constraints, the scope of this project had to be limited to investigation of the rat livers.

The next step in the translational project is to investigate serum levels of FGF21, and expression of FGF21 receptors in the heart and brain of the rats, and to perform the same tests in the female Sprague-Dawley rats. If it is found that serum levels and mRNA levels of the FGF21 and/or the β-klotho receptor is increased, that makes a strong case for FGF21 as a mediator of inter-organ crosstalk.

In the longer term, the goal is to discover non-invasive early biomarkers of people at risk for metabolic disease and complications; mechanisms connecting MAFLD and multi-organ diseases, thus improving the chances of successfully making effective pharmaceutical interventions; which in turn will strengthen the evidence base necessary to influence public health policy and motivate people to live healthier.

5 Conclusion

In conclusion, the results from this master's project demonstrate that an experimental rat model where 15% fructose is administered to the drinking water of the intervention group, increases body weight, liver weight, fat mass, systolic blood pressure, hepatic steatosis, hepatic triglyceride content, and hepatic expression of *Fgf21* and *Atf4* mRNA, while decreasing hepatic expression of *Pdk4* mRNA, in the fructose group compared to the control group. Taken together, all methods employed in this project points toward a state of fructose-induced metabolic dysfunction and arguably an early phase MAFLD.

References

1. Malik VS, Hu FB. Fructose and Cardiometabolic Health. Journal of the American College of Cardiology. 2015 Oct;66(14):1615–24.
2. Stanhope KL. Sugar consumption, metabolic disease and obesity: The state of the controversy. Critical Reviews in Clinical Laboratory Sciences. 2016 Jan 2;53(1):52–67.
3. Grembecka M. Natural sweeteners in a human diet. Rocz Panstw Zakl Hig. 2015;66(3):195–202.
4. Saraiva A, Carrascosa C, Raheem D, Ramos F, Raposo A. Natural Sweeteners: The Relevance of Food Naturalness for Consumers, Food Security Aspects, Sustainability and Health Impacts. IJERPH. 2020 Aug 28;17(17):6285.
5. Rippe JM, Angelopoulos TJ. Sucrose, High-Fructose Corn Syrup, and Fructose, Their Metabolism and Potential Health Effects: What Do We Really Know? Advances in Nutrition. 2013 Mar;4(2):236–45.
6. Le MT, Frye RF, Rivard CJ, Cheng J, McFann KK, Segal MS, et al. Effects of high-fructose corn syrup and sucrose on the pharmacokinetics of fructose and acute metabolic and hemodynamic responses in healthy subjects. Metabolism. 2012 May;61(5):641–51.
7. Stanhope KL, Griffen SC, Bair BR, Swarbrick MM, Keim NL, Havel PJ. Twenty-four-hour endocrine and metabolic profiles following consumption of high-fructose corn syrup-, sucrose-, fructose-, and glucose-sweetened beverages with meals. The American Journal of Clinical Nutrition. 2008 May;87(5):1194–203.
8. Taskinen, Packard, Borén. Dietary Fructose and the Metabolic Syndrome. Nutrients. 2019 Aug 22;11(9):1987.
9. Sutton CA, Stratton M, L'Insalata AM, Fazzino TL. Ultraprocessed, hyper-palatable, and high energy density foods: Prevalence and distinction across 30 years in the UNITED STATES. Obesity. 2023 Oct 4;oby.23897.
10. Popkin BM. The nutrition transition in low-income countries: an emerging crisis. Nutr Rev. 1994 Sep;52(9):285–98.
11. Popkin BM, Adair LS, Ng SW. Global nutrition transition and the pandemic of obesity in developing countries. Nutr Rev. 2012 Jan;70(1):3–21.
12. Johnson RJ, Perez-Pozo SE, Sautin YY, Manitius J, Sanchez-Lozada LG, Feig DI, et al. Hypothesis: Could Excessive Fructose Intake and Uric Acid Cause Type 2 Diabetes? Endocrine Reviews. 2009 Feb 1;30(1):96–116.
13. Jung S, Bae H, Song WS, Jang C. Dietary Fructose and Fructose-Induced Pathologies. Annu Rev Nutr. 2022 Aug 22;42(1):45–66.
14. Stricker S, Rudloff S, Geier A, Steveling A, Roeb E, Zimmer KP. Fructose Consumption—Free Sugars and Their Health Effects. Deutsches Ärzteblatt international [Internet]. 2021 Feb 5 [cited 2023 Dec 27]; Available from: https://www.aerzteblatt.de/10.3238/arztebl.m2021.0010
15. Lowette K, Roosen L, Tack J, Vanden Berghe P. Effects of High-Fructose Diets on Central Appetite Signaling and Cognitive Function. Front Nutr [Internet]. 2015 Mar 4 [cited 2024 Feb 1];2. Available from: http://journal.frontiersin.org/Article/10.3389/fnut.2015.00005/abstract
16. Merino B, Fernández-Díaz CM, Cózar-Castellano I, Perdomo G. Intestinal Fructose and Glucose Metabolism in Health and Disease. Nutrients. 2019 Dec 29;12(1):94.
17. Ferraris RP, Choe JY, Patel CR. Intestinal Absorption of Fructose. Annu Rev Nutr. 2018 Aug 21;38:41–67.
18. Jang C, Hui S, Lu W, Cowan AJ, Morscher RJ, Lee G, et al. The Small Intestine Converts Dietary Fructose into Glucose and Organic Acids. Cell Metab. 2018 Feb 6;27(2):351-361.e3.
19. Mayes P. Intermediary metabolism of fructose. The American Journal of Clinical

Nutrition. 1993 Nov;58(5):754S-765S.
20. Hannou SA, Haslam DE, McKeown NM, Herman MA. Fructose metabolism and metabolic disease. Journal of Clinical Investigation. 2018 Feb 1;128(2):545–55.
21. Schaffner F, Thaler H. Nonalcoholic fatty liver disease. Prog Liver Dis. 1986;8:283–98.
22. Cai J, Zhang XJ, Ji YX, Zhang P, She ZG, Li H. Nonalcoholic Fatty Liver Disease Pandemic Fuels the Upsurge in Cardiovascular Diseases. Circ Res. 2020 Feb 28;126(5):679–704.
23. Khan MAB, Hashim MJ, King JK, Govender RD, Mustafa H, Al Kaabi J. Epidemiology of Type 2 Diabetes - Global Burden of Disease and Forecasted Trends. J Epidemiol Glob Health. 2020 Mar;10(1):107–11.
24. Seidell JC, Halberstadt J. The Global Burden of Obesity and the Challenges of Prevention. Ann Nutr Metab. 2015;66(Suppl. 2):7–12.
25. Lonardo A, Leoni S, Alswat KA, Fouad Y. History of Nonalcoholic Fatty Liver Disease. Int J Mol Sci. 2020 Aug 16;21(16):5888.
26. Eslam M, Sanyal AJ, George J, Sanyal A, Neuschwander-Tetri B, Tiribelli C, et al. MAFLD: A Consensus-Driven Proposed Nomenclature for Metabolic Associated Fatty Liver Disease. Gastroenterology. 2020 May;158(7):1999-2014.e1.
27. Eslam M, Newsome PN, Sarin SK, Anstee QM, Targher G, Romero-Gomez M, et al. A new definition for metabolic dysfunction-associated fatty liver disease: An international expert consensus statement. Journal of Hepatology. 2020 Jul;73(1):202–9.
28. Targher G. What's Past Is Prologue: History of Nonalcoholic Fatty Liver Disease. Metabolites. 2020 Oct 8;10(10):397.
29. Drożdż K, Nabrdalik K, Hajzler W, Kwiendacz H, Gumprecht J, Lip GYH. Metabolic-Associated Fatty Liver Disease (MAFLD), Diabetes, and Cardiovascular Disease: Associations with Fructose Metabolism and Gut Microbiota. Nutrients. 2021 Dec 27;14(1):103.
30. Lin S, Huang J, Wang M, Kumar R, Liu Y, Liu S, et al. Comparison of MAFLD and NAFLD diagnostic criteria in real world. Liver Int. 2020 Sep;40(9):2082–9.
31. Lanzaro F, Guarino S, D'Addio E, Salvatori A, D'Anna JA, Marzuillo P, et al. Metabolic-associated fatty liver disease from childhood to adulthood: State of art and future directions. WJH. 2022 Jun 27;14(6):1087–98.
32. Campbell I. Liver: functional anatomy and blood supply. Anaesthesia & Intensive Care Medicine. 2006 Feb;7(2):49–51.
33. Gelman S, Mushlin PS, Weiskopf RB. Catecholamine-induced Changes in the Splanchnic Circulation Affecting Systemic Hemodynamics. Anesthesiology. 2004 Feb 1;100(2):434–9.
34. Vaja R, Rana M. Drugs and the liver. Anaesthesia & Intensive Care Medicine. 2020 Oct;21(10):517–23.
35. Braet F, Wisse E. Structural and functional aspects of liver sinusoidal endothelial cell fenestrae: a review. Comp Hepatol. 2002;1(1):1.
36. Cunningham RP, Porat-Shliom N. Liver Zonation – Revisiting Old Questions With New Technologies. Front Physiol. 2021 Sep 9;12:732929.
37. Sanz-García C, Fernández-Iglesias A, Gracia-Sancho J, Arráez-Aybar LA, Nevzorova YA, Cubero FJ. The Space of Disse: The Liver Hub in Health and Disease. Livers. 2021 Feb 3;1(1):3–26.
38. Geerts A. History, Heterogeneity, Developmental Biology, and Functions of Quiescent Hepatic Stellate Cells. Semin Liver Dis. 2001;21(03):311–36.
39. Kamm DR, McCommis KS. Hepatic stellate cells in physiology and pathology. The Journal of Physiology. 2022 Apr;600(8):1825–37.

40. Wisse E, Braet F, Dianzhong Luo, De Zanger R, Jans D, Crabbe E, et al. Structure and Function of Sinusoidal Lining Cells in the Liver. Toxicol Pathol. 1996 Jan;24(1):100–11.
41. Haas JT, Francque S, Staels B. Pathophysiology and Mechanisms of Nonalcoholic Fatty Liver Disease. Annu Rev Physiol. 2016 Feb 10;78(1):181–205.
42. Judge A, Dodd MS. Metabolism. Essays in Biochemistry. 2020 Oct 8;64(4):607–47.
43. Han HS, Kang G, Kim JS, Choi BH, Koo SH. Regulation of glucose metabolism from a liver-centric perspective. Exp Mol Med. 2016 Mar 11;48(3):e218–e218.
44. Sharabi K, Tavares CDJ, Puigserver P. Regulation of Hepatic Metabolism, Recent Advances, and Future Perspectives. Curr Diab Rep. 2019 Oct;19(10):98.
45. Carthew RW. Gene Regulation and Cellular Metabolism: An Essential Partnership. Trends in Genetics. 2021 Apr;37(4):389–400.
46. Mercadante AA, Dimri M, Mohiuddin SS. Biochemistry, Replication and Transcription. In: StatPearls [Internet]. Treasure Island (FL): StatPearls Publishing; 2024 [cited 2024 May 8]. Available from: http://www.ncbi.nlm.nih.gov/books/NBK540152/
47. Hoerter JE, Ellis SR. Biochemistry, Protein Synthesis. In: StatPearls [Internet]. Treasure Island (FL): StatPearls Publishing; 2024 [cited 2024 May 8]. Available from: http://www.ncbi.nlm.nih.gov/books/NBK545161/
48. Chen L, Kashina A. Post-translational Modifications of the Protein Termini. Front Cell Dev Biol. 2021 Jul 29;9:719590.
49. Latchman DS. Transcription factors: an overview. Int J Exp Pathol. 1993 Oct;74(5):417–22.
50. Mirkovitch J. A Few Glances at the Function of Chromatin and Nuclear Higher-Order Structure in Transcription Regulation. In: Xanthopoulos KG, editor. Gene Therapy [Internet]. Berlin, Heidelberg: Springer Berlin Heidelberg; 1998 [cited 2024 Apr 27]. p. 1–16. Available from: http://link.springer.com/10.1007/978-3-642-72160-1_1
51. Gibney ER, Nolan CM. Epigenetics and gene expression. Heredity. 2010 Jul;105(1):4–13.
52. JCI Insight - Gene Nomenclature and Style [Internet]. [cited 2024 May 12]. Available from: https://insight.jci.org/kiosks/publish/genestyle
53. Karra P, Winn M, Pauleck S, Bulsiewicz-Jacobsen A, Peterson L, Coletta A, et al. Metabolic dysfunction and obesity-related cancer: Beyond obesity and metabolic syndrome. Obesity. 2022 Jul;30(7):1323–34.
54. Bertola A, Bonnafous S, Anty R, Patouraux S, Saint-Paul MC, Iannelli A, et al. Hepatic Expression Patterns of Inflammatory and Immune Response Genes Associated with Obesity and NASH in Morbidly Obese Patients. Gimble JM, editor. PLoS ONE. 2010 Oct 22;5(10):e13577.
55. DiStefano JK. Fructose-mediated effects on gene expression and epigenetic mechanisms associated with NAFLD pathogenesis. Cell Mol Life Sci. 2020 Jun;77(11):2079–90.
56. Donnelly KL, Smith CI, Schwarzenberg SJ, Jessurun J, Boldt MD, Parks EJ. Sources of fatty acids stored in liver and secreted via lipoproteins in patients with nonalcoholic fatty liver disease. J Clin Invest. 2005 May;115(5):1343–51.
57. Schuppan D, Afdhal NH. Liver cirrhosis. The Lancet. 2008 Mar;371(9615):838–51.
58. Engelmann C, Clària J, Szabo G, Bosch J, Bernardi M. Pathophysiology of decompensated cirrhosis: Portal hypertension, circulatory dysfunction, inflammation, metabolism and mitochondrial dysfunction. Journal of Hepatology. 2021 Jul;75:S49–66.
59. Oliver TI, Sharma B, John S. Portal Hypertension. In: StatPearls [Internet]. Treasure Island (FL): StatPearls Publishing; 2024 [cited 2024 May 8]. Available from: http://www.ncbi.nlm.nih.gov/books/NBK507718/
60. Jensen-Cody SO, Potthoff MJ. Hepatokines and metabolism: Deciphering

communication from the liver. Molecular Metabolism. 2021 Feb;44:101138.
61. Castillo-Armengol J, Fajas L, Lopez-Mejia IC. Inter-organ communication: a gatekeeper for metabolic health. EMBO Reports. 2019 Sep;20(9):e47903.
62. Zhang X, Ji X, Wang Q, Li JZ. New insight into inter-organ crosstalk contributing to the pathogenesis of non-alcoholic fatty liver disease (NAFLD). Protein Cell. 2018 Feb;9(2):164–77.
63. Itier R, Guillaume M, Ricci J, Roubille F, Delarche N, Picard F, et al. Non-alcoholic fatty liver disease and heart failure with preserved ejection fraction: from pathophysiology to practical issues. ESC Heart Failure. 2021 Apr;8(2):789–98.
64. Chou RH, Huang PH, Hsu CY, Chang CC, Leu HB, Huang CC, et al. Circulating Fibroblast Growth Factor 21 is Associated with Diastolic Dysfunction in Heart Failure Patients with Preserved Ejection Fraction. Sci Rep. 2016 Sep 21;6(1):33953.
65. Wu CT, Chaffin AT, Ryan KK. Fibroblast Growth Factor 21 Facilitates the Homeostatic Control of Feeding Behavior. JCM. 2022 Jan 24;11(3):580.
66. Sommakia S, Almaw NH, Lee SH, Ramadurai DKA, Taleb I, Kyriakopoulos CP, et al. FGF21 (Fibroblast Growth Factor 21) Defines a Potential Cardiohepatic Signaling Circuit in End-Stage Heart Failure. Circ: Heart Failure. 2022 Mar;15(3):e008910.
67. Steensels S, Qiao J, Ersoy BA. Transcriptional Regulation in Non-Alcoholic Fatty Liver Disease. Metabolites. 2020 Jul 9;10(7):283.
68. Régnier M, Carbinatti T, Parlati L, Benhamed F, Postic C. The role of ChREBP in carbohydrate sensing and NAFLD development. Nat Rev Endocrinol. 2023 Jun;19(6):336–49.
69. Ortega-Prieto P, Postic C. Carbohydrate Sensing Through the Transcription Factor ChREBP. Front Genet. 2019 Jun 4;10:472.
70. Ferré P, Foufelle F. Hepatic steatosis: a role for *de novo* lipogenesis and the transcription factor SREBP-1c. Diabetes Obesity Metabolism. 2010 Oct;12(s2):83–92.
71. Xu X, So JS, Park JG, Lee AH. Transcriptional Control of Hepatic Lipid Metabolism by SREBP and ChREBP. Semin Liver Dis. 2013 Nov 12;33(04):301–11.
72. Montaigne D, Butruille L, Staels B. PPAR control of metabolism and cardiovascular functions. Nat Rev Cardiol. 2021 Dec;18(12):809–23.
73. Souza-Mello V. Peroxisome proliferator-activated receptors as targets to treat non-alcoholic fatty liver disease. WJH. 2015;7(8):1012.
74. Changizi Z, Kajbaf F, Moslehi A. An Overview of the Role of Peroxisome Proliferator-activated Receptors in Liver Diseases. J Clin Transl Hepatol. 2023 Dec 28;11(7):1542–52.
75. Finck BN. PGC-1 coactivators: inducible regulators of energy metabolism in health and disease. Journal of Clinical Investigation. 2006 Mar 1;116(3):615–22.
76. Kohjima M, Enjoji M, Higuchi N, Kato M, Kotoh K, Yoshimoto T, et al. Re-evaluation of fatty acid metabolism-related gene expression in nonalcoholic fatty liver disease. Int J Mol Med [Internet]. 2007 Sep 1 [cited 2024 Apr 18]; Available from: http://www.spandidos-publications.com/10.3892/ijmm.20.3.351
77. Weber M, Mera P, Casas J, Salvador J, Rodríguez A, Alonso S, et al. Liver CPT1A gene therapy reduces diet-induced hepatic steatosis in mice and highlights potential lipid biomarkers for human NAFLD. FASEB j. 2020 Sep;34(9):11816–37.
78. Wang X, Shen X, Yan Y, Li H. Pyruvate dehydrogenase kinases (PDKs): an overview toward clinical applications. Bioscience Reports. 2021 Apr 30;41(4):BSR20204402.
79. Jeon J, Thoudam T, Choi EJ, Kim M, Harris RA, Lee I. Loss of metabolic flexibility as a result of overexpression of pyruvate dehydrogenase kinases in muscle, liver and the immune system: Therapeutic targets in metabolic diseases. J of Diabetes Invest. 2021 Jan;12(1):21–31.

80. Duan Y, Pan X, Luo J, Xiao X, Li J, Bestman PL, et al. Association of Inflammatory Cytokines With Non-Alcoholic Fatty Liver Disease. Front Immunol. 2022 May 6;13:880298.
81. Faheem S, Saeed N, El-naga R, Azab S. Non alcoholic fatty liver disease: pathogenesis, role of (TNF-α, IL-6) in hepatic inflammation and future potential nutraceutical treatment. Archives of Pharmaceutical Sciences Ain Shams University. 2019 Jun 1;3(2):154–69.
82. Heyens LJM, Busschots D, Koek GH, Robaeys G, Francque S. Liver Fibrosis in Non-alcoholic Fatty Liver Disease: From Liver Biopsy to Non-invasive Biomarkers in Diagnosis and Treatment. Front Med. 2021 Apr 14;8:615978.
83. Zhang XQ. Role of endoplasmic reticulum stress in the pathogenesis of nonalcoholic fatty liver disease. WJG. 2014;20(7):1768.
84. Lebeaupin C, Vallée D, Hazari Y, Hetz C, Chevet E, Bailly-Maitre B. Endoplasmic reticulum stress signalling and the pathogenesis of non-alcoholic fatty liver disease. Journal of Hepatology. 2018 Oct;69(4):927–47.
85. Toop C, Gentili S. Fructose Beverage Consumption Induces a Metabolic Syndrome Phenotype in the Rat: A Systematic Review and Meta-Analysis. Nutrients. 2016 Sep 20;8(9):577.
86. Meng Q, Ying Z, Noble E, Zhao Y, Agrawal R, Mikhail A, et al. Systems Nutrigenomics Reveals Brain Gene Networks Linking Metabolic and Brain Disorders. EBioMedicine. 2016 May;7:157–66.
87. Chan JKC. The Wonderful Colors of the Hematoxylin–Eosin Stain in Diagnostic Surgical Pathology. Int J Surg Pathol. 2014 Feb;22(1):12–32.
88. Kandyala R, Raghavendra SP, Rajasekharan S. Xylene: An overview of its health hazards and preventive measures. J Oral Maxillofac Pathol. 2010;14(1):1.
89. Mehlem A, Hagberg CE, Muhl L, Eriksson U, Falkevall A. Imaging of neutral lipids by oil red O for analyzing the metabolic status in health and disease. Nat Protoc. 2013 Jun;8(6):1149–54.
90. Bankhead P, Loughrey MB, Fernández JA, Dombrowski Y, McArt DG, Dunne PD, et al. QuPath: Open source software for digital pathology image analysis. Sci Rep. 2017 Dec 4;7(1):16878.
91. Liang W, Menke AL, Driessen A, Koek GH, Lindeman JH, Stoop R, et al. Establishment of a General NAFLD Scoring System for Rodent Models and Comparison to Human Liver Pathology. Sookoian SC, editor. PLoS ONE. 2014 Dec 23;9(12):e115922.
92. Cobb M. 60 years ago, Francis Crick changed the logic of biology. PLoS Biol. 2017 Sep 18;15(9):e2003243.
93. Xie F, Wang J, Zhang B. RefFinder: a web-based tool for comprehensively analyzing and identifying reference genes. Funct Integr Genomics. 2023 Jun;23(2):125.
94. Barde M, Barde P. What to use to express the variability of data: Standard deviation or standard error of mean? Perspect Clin Res. 2012;3(3):113.
95. Chen HH, Chu CH, Wen SW, Lai CC, Cheng PW, Tseng CJ. Excessive Fructose Intake Impairs Baroreflex Sensitivity and Led to Elevated Blood Pressure in Rats. Nutrients. 2019 Oct 25;11(11):2581.
96. Lodge M, Scheidemantle G, Adams VR, Cottam MA, Richard D, Breuer D, et al. Fructose regulates the pentose phosphate pathway and induces an inflammatory and resolution phenotype in Kupffer cells. Sci Rep. 2024 Feb 18;14(1):4020.
97. Fang T, Wang H, Pan X, Little PJ, Xu S, Weng J. Mouse models of nonalcoholic fatty liver disease (NAFLD): pathomechanisms and pharmacotherapies. Int J Biol Sci. 2022;18(15):5681–97.
98. Dushay JR, Toschi E, Mitten EK, Fisher FM, Herman MA, Maratos-Flier E. Fructose ingestion acutely stimulates circulating FGF21 levels in humans. Molecular Metabolism.

2015 Jan;4(1):51–7.
99. Fisher ffolliott M, Kim M, Doridot L, Cunniff JC, Parker TS, Levine DM, et al. A critical role for ChREBP-mediated FGF21 secretion in hepatic fructose metabolism. Molecular Metabolism. 2017 Jan;6(1):14–21.
100. Keinicke H, Sun G, Mentzel CMJ, Fredholm M, John LM, Andersen B, et al. FGF21 regulates hepatic metabolic pathways to improve steatosis and inflammation. Endocrine Connections. 2020 Aug;9(8):755–68.
101. Raptis DD, Mantzoros CS, Polyzos SA. Fibroblast Growth Factor-21 as a Potential Therapeutic Target of Nonalcoholic Fatty Liver Disease. TCRM. 2023 Jan;Volume 19:77–96.
102. Henkel A, Green R. The Unfolded Protein Response in Fatty Liver Disease. Semin Liver Dis. 2013 Nov 12;33(04):321–9.
103. Xiao G, Zhang T, Yu S, Lee S, Calabuig-Navarro V, Yamauchi J, et al. ATF4 Protein Deficiency Protects against High Fructose-induced Hypertriglyceridemia in Mice. Journal of Biological Chemistry. 2013 Aug;288(35):25350–61.
104. Zhang M, Zhao Y, Li Z, Wang C. Pyruvate dehydrogenase kinase 4 mediates lipogenesis and contributes to the pathogenesis of nonalcoholic steatohepatitis. Biochemical and Biophysical Research Communications. 2018 Jan;495(1):582–6.
105. Henkel J, Buchheim-Dieckow K, Castro JP, Laeger T, Wardelmann K, Kleinridders A, et al. Reduced Oxidative Stress and Enhanced FGF21 Formation in Livers of Endurance-Exercised Rats with Diet-Induced NASH. Nutrients. 2019 Nov 8;11(11):2709.
106. García-Berumen CI, Ortiz-Avila O, Vargas-Vargas MA, del Rosario-Tamayo BA, Guajardo-López C, Saavedra-Molina A, et al. The severity of rat liver injury by fructose and high fat depends on the degree of respiratory dysfunction and oxidative stress induced in mitochondria. Lipids Health Dis. 2019 Dec;18(1):78.
107. Slaoui M, Bauchet AL, Fiette L. Tissue Sampling and Processing for Histopathology Evaluation. In: Gautier JC, editor. Drug Safety Evaluation [Internet]. New York, NY: Springer New York; 2017 [cited 2024 May 1]. p. 101–14. (Methods in Molecular Biology; vol. 1641). Available from: http://link.springer.com/10.1007/978-1-4939-7172-5_4
108. Liyanage S, Dassanayake RS, Bouyanfif A, Rajakaruna E, Ramalingam L, Moustaid-Moussa N, et al. Optimization and validation of cryostat temperature conditions for trans-reflectance mode FTIR microspectroscopic imaging of biological tissues. MethodsX. 2017;4:118–27.
109. Lattouf R, Younes R, Lutomski D, Naaman N, Godeau G, Senni K, et al. Picrosirius Red Staining: A Useful Tool to Appraise Collagen Networks in Normal and Pathological Tissues. J Histochem Cytochem. 2014 Oct;62(10):751–8.
110. Junqueira LCU, Bignolas G, Brentani RR. Picrosirius staining plus polarization microscopy, a specific method for collagen detection in tissue sections. Histochem J. 1979 Jul;11(4):447–55.
111. Brunt EM, Janney CG, Di Bisceglie AM, Neuschwander-Tetri BA, Bacon BR. Nonalcoholic Steatohepatitis: A Proposal for Grading and Staging The Histological Lesions. American Journal of Gastroenterology. 1999 Sep;94(9):2467–74.
112. Kleiner DE, Brunt EM, Van Natta M, Behling C, Contos MJ, Cummings OW, et al. Design and validation of a histological scoring system for nonalcoholic fatty liver disease. Hepatology. 2005 Jun;41(6):1313–21.
113. Seyhan AA. Lost in translation: the valley of death across preclinical and clinical divide – identification of problems and overcoming obstacles. transl med commun. 2019 Dec;4(1):18.
114. Fang E, Liu X, Li M, Zhang Z, Song L, Zhu B, et al. Advances in COVID-19 mRNA vaccine development. Signal Transduct Target Ther. 2022 Mar 23;7(1):94.
115. Zezos P, Renner EL. Liver transplantation and non-alcoholic fatty liver disease. World

J Gastroenterol. 2014 Nov 14;20(42):15532–8.
116. Pasquali P. The importance of animal models in research. Research in Veterinary Science. 2018 Jun;118:144–5.
117. Sengupta P. The Laboratory Rat: Relating Its Age With Human's. Int J Prev Med. 2013 Jun;4(6):624–30.
118. Demetrius L. Of mice and men: When it comes to studying ageing and the means to slow it down, mice are not just small humans. EMBO Reports [Internet]. 2005 Jul [cited 2024 Apr 25];6(S1). Available from: https://www.embopress.org/doi/10.1038/sj.embor.7400422
119. Kowalski GM, Bruce CR. The regulation of glucose metabolism: implications and considerations for the assessment of glucose homeostasis in rodents. American Journal of Physiology-Endocrinology and Metabolism. 2014 Nov 15;307(10):E859–71.
120. Agoston DV. How to Translate Time? The Temporal Aspect of Human and Rodent Biology. Front Neurol [Internet]. 2017 Mar 17 [cited 2024 May 1];8. Available from: http://journal.frontiersin.org/article/10.3389/fneur.2017.00092/full
121. Ghasemi A, Jeddi S, Kashfi K. The laboratory rat: age and body weight matter. EXCLI Journal; 20:Doc1431; ISSN 1611-2156 [Internet]. 2021 [cited 2024 May 1]; Available from: https://www.excli.de/index.php/excli/article/view/4072
122. Clemente-Suárez VJ, Beltrán-Velasco AI, Redondo-Flórez L, Martín-Rodríguez A, Tornero-Aguilera JF. Global Impacts of Western Diet and Its Effects on Metabolism and Health: A Narrative Review. Nutrients. 2023 Jun 14;15(12):2749.
123. Fuller KNZ, Thyfault JP. Barriers in translating preclinical rodent exercise metabolism findings to human health. Journal of Applied Physiology. 2021 Jan 1;130(1):182–92.
124. Poole S, Stephenson JD. BODY TEMPERATURE REGULATION AND THERMONEUTRALITY IN RATS. Exp Physiol. 1977 Apr 7;62(2):143–9.
125. Hankenson FC, Marx JO, Gordon CJ, David JM. Effects of Rodent Thermoregulation on Animal Models in the Research Environment. comp med. 2018 Dec 1;68(6):425–38.
126. Herrero L, Valcarcel L, Da Silva CA, Albert N, Diez-Noguera A, Cambras T, et al. Altered Circadian Rhythm and Metabolic Gene Profile in Rats Subjected to Advanced Light Phase Shifts. Gamble KL, editor. PLoS ONE. 2015 Apr 2;10(4):e0122570.
127. Mauvais-Jarvis F, Arnold AP, Reue K. A Guide for the Design of Pre-clinical Studies on Sex Differences in Metabolism. Cell Metabolism. 2017 Jun;25(6):1216–30.
128. Zhou W, Zeng G, Lyu C, Kou F, Zhang S, Wei H. The Effect of Exhaustive Exercise on Plasma Metabolic Profiles of Male and Female Rats. J Sports Sci Med. 2019 Jun;18(2):253–63.
129. Gao Y, Yu Y, Qin W, Fan N, Qi Y, Chen H, et al. Uricase-deficient rats with similarly stable serum uric acid to human's are sensitive model animals for studying hyperuricemia. Joles JA, editor. PLoS ONE. 2022 Mar 3;17(3):e0264696.
130. Bland JM, Altman DG. Statistics notes: Bayesians and frequentists. BMJ. 1998 Oct 24;317(7166):1151–60.
131. Perezgonzalez JD. Fisher, Neyman-Pearson or NHST? A tutorial for teaching data testing. Front Psychol [Internet]. 2015 Mar 3 [cited 2024 May 5];6. Available from: http://journal.frontiersin.org/Article/10.3389/fpsyg.2015.00223/abstract
132. Nuzzo R. Scientific method: Statistical errors. Nature. 2014 Feb 13;506(7487):150–2.
133. Ranganathan P, Pramesh C, Buyse M. Common pitfalls in statistical analysis: Clinical versus statistical significance. Perspect Clin Res. 2015;6(3):169.
134. Kiani AK, Pheby D, Henehan G, Brown R, Sieving P, Sykora P, et al. Ethical considerations regarding animal experimentation. Journal of Preventive Medicine and Hygiene. 2022 Oct 17;Vol. 63 No. 2S3:E255 Pages.
135. Mukherjee P, Roy S, Ghosh D, Nandi SK. Role of animal models in biomedical research: a review. Lab Anim Res. 2022 Dec;38(1):18.

136. Greenland S. Randomization, Statistics, and Causal Inference: Epidemiology. 1990 Nov;1(6):421–9.

Appendices

Appendix A. Summary Statistics

Table A1: Summary statistics of the control group

Variable	Min	1st Qua	Mean	Median	3rd Qua	Max	N
BW	620	654	675	676	691	717	12
LW	16	18	19	19	19	21	12
FM	0.02	7.6	12	10	12	29	12
TG	0.63	0.85	1.2	1.1	1.4	1.8	11
ORO	0.03	0.035	0.3	0.06	0.35	1.6	11
PSR	0.15	1.7	3.8	3	6.2	8.7	8
SBP	93	106	120	123	131	139	12

Table A2: Summary statistics of the fructose group

Variable	Min	1st Qua	Mean	Median	3rd Qua	Max	N
BW	704	746	766	769	791	827	12
LW	24	25	26	26	27	30	12
FM	8.2	14	28	27	39	52	12
TG	0.75	1.4	1.8	1.8	2	3	12
ORO	0.34	1.4	4.1	2.8	3.8	15	11
PSR	0.09	0.83	3.3	1.4	4.7	10	11
SBP	112	126	135	137	142	155	12

Appendix B. Individual Level Data

Table B1: Individual level data from the fructose and control group. Data collected at the end of the 16-week intervention (BW, LW, FM, SBP) or from tissue that has been stored for approximately 1 year (TG, ORO, PSR). Missing values in ORO and PSR is due to tissue damage that has occured during the preparation, sectioning, or staining phase, as adressed in the limitations. *BW = body weight, LW = liver weight, FM = fat mass, TG = triglycerides, ORO = Oil Red O, PSR = Picro Sirius Red, SBP = systolic blood pressure.*

Group	ID	BW (g)	LW (g)	FM (g)	TG (nmol)	ORO (%)	PSR (%)	SBP
Fructose	A1	783,00	26,32	37,1	1,08	1,77	0,7	137
Fructose	A2	769,00	25,76	100,7	0,75	2,89	3,6	124
Fructose	C1	740,00	24,50	93,5	1,67	3,17	5,84	137
Fructose	C2	720,00	25,45	62,2	1,94	4,35	10,17	136
Fructose	F1	766,00	26,44	81,2	1,87	1,91	1,4	137
Fructose	F2	781,00	23,60	71,7	1,83	0,34	3,44	141
Fructose	I1	723,00	28,59	47,8	1,14	0,38	0,09	112
Fructose	I2	736,00	29,67	87,1	2,97	15,31	1,33	126
Fructose	J1	682,00	28,23	50,8	1,55	2,78	0,96	126
Fructose	J2	678,00	24,33	21,8	2,26	0,98	8,69	155
Fructose	L1	746,00	27,20	43,4	2,89		0,18	145
Fructose	L2	705,00	24,85	15,2	1,60	10,74		143
Control	B1	680,00	21,21	19,64	0,63	0,04		137
Control	B2	640,00	18,82	19,7	1,80	1,61		124
Control	D1	660,00	18,92	23,55	1,32	0,05	3,82	101
Control	D2	649,00	16,22	1,9	1,07	0,03	6,11	122
Control	E1	692,00	19,40	23,81			1,93	107
Control	E2	632,00	18,56	14,4	0,77	0,03	0,15	126
Control	G1	705,00	19,24	23,47	1,25	0,13	1,1	133
Control	G2	656,00	20,66	28,37	1,13	0,06	8,66	139
Control	H1	659,00	18,96	26,73	1,60	0,03		102
Control	H2	649,00	17,72	11,47	0,67	0,59	2,15	122
Control	K1	609,00	17,62	29,1	0,94	0,55	6,52	130
Control	K2	659,00	17,91	1	1,57	0,15		93

Table B2: Individual level data from the PSR staining. Three areas of 250000 µm^2 were randomly chosen from each slide, and the average amount of stain per area was used to statistical analysis. *Fr = fructose, Cr = control.*

Picro Sirius Red					
Sample	**ROI**	**PSR area µm²**	**Total area µm²**	**% area stained**	
A1-L-PSR.vsi - 20x_02	Rectangle	1790,2	250000	0,72 %	
A1-L-PSR.vsi - 20x_02	Rectangle	2668,2244	250000	1,07 %	
A1-L-PSR.vsi - 20x_02	Rectangle	800,2209	250000	0,32 %	
Average		1752,88	250000	0,70 %	**Fr**
C1-L-PSR.vsi - 20x_01	Rectangle	16450,1191	250000	6,58 %	
C1-L-PSR.vsi - 20x_01	Rectangle	15903,7295	250000	6,36 %	
C1-L-PSR.vsi - 20x_01	Rectangle	11434,7441	250000	4,57 %	
Average		14596,20	250000	5,84 %	**Fr**
D2-L-PSR.vsi - 20x	Rectangle	11679,0703	250000	4,67 %	
D2-L-PSR.vsi - 20x	Rectangle	9727,5127	250000	3,89 %	
D2-L-PSR.vsi - 20x	Rectangle	24431,3223	250000	9,77 %	
Average		15279,30	250000	6,11 %	**Cr**
E1-L-PSR.vsi - 20x	Rectangle	6198,2793	250000	2,48 %	
E1-L-PSR.vsi - 20x	Rectangle	6406,3438	250000	2,56 %	
E1-L-PSR.vsi - 20x	Rectangle	1873,2843	250000	0,75 %	
Average		4825,97	250000	1,93 %	**Cr**
F1-L-PSR.vsi - 20x	Rectangle	4779,9673	250000	1,91 %	
F1-L-PSR.vsi - 20x	Rectangle	3691,4133	250000	1,48 %	
F1-L-PSR.vsi - 20x	Rectangle	2022,2036	250000	0,81 %	
Average		3497,86	250000	1,40 %	**Fr**
G1-L-PSR.vsi - 20x	Rectangle	1720,8445	250000	0,69 %	
G1-L-PSR.vsi - 20x	Rectangle	1041,2611	250000	0,42 %	
G1-L-PSR.vsi - 20x	Rectangle	5493,2305	250000	2,20 %	
Average		2751,78	250000	1,10 %	**Cr**
I2-L-PSR.vsi - 20x	Rectangle	5086,6069	250000	2,03 %	
I2-L-PSR.vsi - 20x	Rectangle	2508,1567	250000	1,00 %	
I2-L-PSR.vsi - 20x	Rectangle	2396,5554	250000	0,96 %	
Average		3330,44	250000	1,33 %	**Fr**
K1-L-PSR.vsi - 20x	Rectangle	12114,5625	250000	4,85 %	
K1-L-PSR.vsi - 20x	Rectangle	15672,0771	250000	6,27 %	
K1-L-PSR.vsi - 20x	Rectangle	21096,7754	250000	8,44 %	
Average		16294,47	250000	6,52 %	**Cr**
A2-L__Rat_Liver_PSR.vsi - 20x	Rectangle	13060,6514	250000	5,22 %	

A2-L__Rat_Liver_PSR.vsi - 20x	Rectangle	4548,5498	250000	1,82 %	
A2-L__Rat_Liver_PSR.vsi - 20x	Rectangle	9427,0928	250000	3,77 %	
Average		9012,10	250000	3,60 %	**Fr**
C2-L__Rat_Liver_PSR.vsi - 20x	Rectangle	20063,6113	250000	8,03 %	
C2-L__Rat_Liver_PSR.vsi - 20x	Rectangle	31030,709	250000	12,41 %	
C2-L__Rat_Liver_PSR.vsi - 20x	Rectangle	25155,2637	250000	10,06 %	
Average		25416,53	250000	10,17 %	**Fr**
D1-L__Rat_Liver_PSR.vsi - 20x	Rectangle	11180,0918	250000	4,47 %	
D1-L__Rat_Liver_PSR.vsi - 20x	Rectangle	6981,7188	250000	2,79 %	
D1-L__Rat_Liver_PSR.vsi - 20x	Rectangle	10452,042	250000	4,18 %	
Average		9537,95	250000	3,82 %	**Cr**
E2-L__Rat_Liver_PSR.vsi - 20x	Rectangle	468,3504	250000	0,19 %	
E2-L__Rat_Liver_PSR.vsi - 20x	Rectangle	223,0855	250000	0,09 %	
E2-L__Rat_Liver_PSR.vsi - 20x	Rectangle	427,6294	250000	0,17 %	
Average		373,02	250000	0,15 %	**Cr**
F2-L__Rat_Liver_PSR.vsi - 20x	Rectangle	9390,3613	250000	3,76 %	
F2-L__Rat_Liver_PSR.vsi - 20x	Rectangle	12353,96	250000	4,94 %	
F2-L__Rat_Liver_PSR.vsi - 20x	Rectangle	4030,4424	250000	1,61 %	
Average		8591,59	250000	3,44 %	**Fr**
G2-L__Rat_Liver_PSR.vsi - 20x	Rectangle	18488,6348	250000	7,40 %	
G2-L__Rat_Liver_PSR.vsi - 20x	Rectangle	7595,3506	250000	3,04 %	
G2-L__Rat_Liver_PSR.vsi - 20x	Rectangle	38833,3008	250000	15,53 %	
Average		21639,10	250000	8,66 %	**Cr**
H2-L__Rat_Liver_PSR.vsi - 20x	Rectangle	3876,3596	250000	1,55 %	
H2-L__Rat_Liver_PSR.vsi - 20x	Rectangle	4646,6558	250000	1,86 %	
H2-L__Rat_Liver_PSR.vsi - 20x	Rectangle	7576,3398	250000	3,03 %	
Average		5366,45	250000	2,15 %	**Cr**
I1-L__Rat_Liver_PSR.vsi - 20x	Rectangle	115,9434	250000	0,05 %	
I1-L__Rat_Liver_PSR.vsi - 20x	Rectangle	396,0618	250000	0,16 %	
I1-L__Rat_Liver_PSR.vsi - 20x	Rectangle	169,9252	250000	0,07 %	
Average		227,31	250000	0,09 %	**Fr**

J1-L__Rat_Liver_PSR.vsi - 20x	Rectangle	1579,6705	250000	0,63 %	
J1-L__Rat_Liver_PSR.vsi - 20x	Rectangle	2946,7	250000	1,18 %	
J1-L__Rat_Liver_PSR.vsi - 20x	Rectangle	2645,2234	250000	1,06 %	
Average		2390,53	250000	0,96 %	**Fr**
J2-L__Rat_Liver_PSR.vsi - 20x	Rectangle	24279,7031	250000	9,71 %	
J2-L__Rat_Liver_PSR.vsi - 20x	Rectangle	20481,3828	250000	8,19 %	
J2-L__Rat_Liver_PSR.vsi - 20x	Rectangle	20429,8652	250000	8,17 %	
Average		21730,32	250000	8,69 %	**Fr**
K2-L__Rat_Liver_PSR.vsi - 20x	Rectangle	21320,6816	250000	8,53 %	
K2-L__Rat_Liver_PSR.vsi - 20x	Rectangle	21899,9297	250000	8,76 %	
K2-L__Rat_Liver_PSR.vsi - 20x	Rectangle	15374,0049	250000	6,15 %	
Average		19531,54	250000	7,81 %	**Cr**
L1-L__Rat_Liver_PSR.vsi - 20x	Rectangle	303,5887	250000	0,12 %	
L1-L__Rat_Liver_PSR.vsi - 20x	Rectangle	468,1157	250000	0,19 %	
L1-L__Rat_Liver_PSR.vsi - 20x	Rectangle	563,992	250000	0,23 %	
Average		445,23	250000	0,18 %	**Fr**

Table B3: Individual level data from the ORO staining. Three areas of 250000 µm^2 were randomly chosen from each slide, and the average amount of stain per area was used to statistical analysis. *Fr = fructose, Cr = control.*

Oil Red O					
Sample	**ROI**	**Oil red area µm²**	**Total area µm²**	**% area stained**	
A1-Liver-ORO	Rectangle	5183,75	250000	2,07 %	
A1-Liver-ORO	Rectangle	1991,07	250000	0,80 %	
A1-Liver-ORO	Rectangle	6126,36	250000	2,45 %	
Average		4433,73	250000	**1,77 %**	**Fr**
B1-Liver-ORO	Rectangle	71,12	250000	0,03 %	
B1-Liver-ORO	Rectangle	146,81	250000	0,06 %	
B1-Liver-ORO	Rectangle	86,84	250000	0,03 %	
Average		101,59	250000	**0,04 %**	**Cr**
D2-Liver-ORO	Rectangle	30,40	250000	0,01 %	
D2-Liver-ORO	Rectangle	40,84	250000	0,02 %	
D2-Liver-ORO	Rectangle	141,30	250000	0,06 %	
Average		70,84	250000	**0,03 %**	**Cr**
F1-Liver-ORO	Rectangle	3314,38	250000	1,33 %	
F1-Liver-ORO	Rectangle	6364,71	250000	2,55 %	
F1-Liver-ORO	Rectangle	4664,21	250000	1,87 %	
Average		4781,10	250000	**1,91 %**	**Fr**
G2-Liver-ORO	Rectangle	354,06	250000	0,14 %	
G2-Liver-ORO	Rectangle	39,08	250000	0,02 %	
G2-Liver-ORO	Rectangle	28,05	250000	0,01 %	
Average		140,40	250000	**0,06 %**	**Cr**
H2-Liver-ORO	Rectangle	3713,98	250000	1,49 %	
H2-Liver-ORO	Rectangle	30,28	250000	0,01 %	
H2-Liver-ORO	Rectangle	708,95	250000	0,28 %	
Average		1484,40	250000	**0,59 %**	**Cr**
I2-Liver-ORO	Rectangle	32585,30	250000	13,03 %	
I2-Liver-ORO	Rectangle	40460,74	250000	16,18 %	
I2-Liver-ORO	Rectangle	41755,65	250000	16,70 %	
Average		38267,23	250000	**15,31 %**	**Fr**
L1-Liver-ORO	Rectangle	13810,03	250000	5,52 %	
L1-Liver-ORO	Rectangle	10814,04	250000	4,33 %	
L1-Liver-ORO	Rectangle	10595,41	250000	4,24 %	

Average		11739,83	250000	**4,70 %**	**Fr**
A2-L-ORO.vsi - 20x	Rectangle	3405,4487	250000	1,36 %	
A2-L-ORO.vsi - 20x	Rectangle	11130,9043	250000	4,45 %	
A2-L-ORO.vsi - 20x	Rectangle	7134,6836	250000	2,85 %	
Average		7223,68	250000	**2,89 %**	**Fr**
B2-L-ORO.vsi - 20x_01	Rectangle	4046,9189	250000	1,62 %	
B2-L-ORO.vsi - 20x_01	Rectangle	4147,6108	250000	1,66 %	
B2-L-ORO.vsi - 20x_01	Rectangle	3886,7275	250000	1,55 %	
Average		4027,09	250000	**1,61 %**	**Cr**
H1-L-ORO.vsi - 20x_01	Rectangle	91,3033	250000	0,04 %	
H1-L-ORO.vsi - 20x_01	Rectangle	109,0241	250000	0,04 %	
H1-L-ORO.vsi - 20x_01	Rectangle	42,0136	250000	0,02 %	
Average		80,78	250000	**0,03 %**	**Fr**
C2-L-ORO.vsi - 20x_02	Rectangle	15034,2969	250000	6,01 %	
C2-L-ORO.vsi - 20x_02	Rectangle	9985,1543	250000	3,99 %	
C2-L-ORO.vsi - 20x_02	Rectangle	7578,7607	250000	3,03 %	
Average		10866,07	250000	**4,35 %**	**Fr**
D1-L-ORO.vsi - 20x_01	Rectangle	178,2644	250000	0,07 %	
D1-L-ORO.vsi - 20x_01	Rectangle	169,8147	250000	0,07 %	
D1-L-ORO.vsi - 20x_01	Rectangle	57,3873	250000	0,02 %	
Average		135,16	250000	**0,05 %**	
E2-L-ORO.vsi - 20x	Rectangle	68,8882	250000	0,03 %	
E2-L-ORO.vsi - 20x	Rectangle	97,6405	250000	0,04 %	
E2-L-ORO.vsi - 20x	Rectangle	27,8135	250000	0,01 %	
Average		64,78	250000	**0,03 %**	
F2-L-ORO.vsi - 20x_01	Rectangle	870,5499	250000	0,35 %	
F2-L-ORO.vsi - 20x_01	Rectangle	638,4189	250000	0,26 %	
F2-L-ORO.vsi - 20x_01	Rectangle	1063,3666	250000	0,43 %	
Average		857,45	250000	**0,34 %**	
G1-L-ORO.vsi - 20x	Rectangle	212,8846	250000	0,09 %	
G1-L-ORO.vsi - 20x	Rectangle	443,1378	250000	0,18 %	
G1-L-ORO.vsi - 20x	Rectangle	325,8988	250000	0,13 %	
Average		327,31	250000	**0,13 %**	
C1-L-ORO.vsi - 20x_01	Rectangle	6661,3853	250000	2,66 %	
C1-L-ORO.vsi - 20x_01	Rectangle	3787,4438	250000	1,51 %	

C1-L-ORO.vsi - 20x_01	Rectangle	13302,4678	250000	5,32 %
Average		7917,10	250000	**3,17 %**
I1-L-ORO.vsi - 20x	Rectangle	680,4326	250000	0,27 %
I1-L-ORO.vsi - 20x	Rectangle	751,6679	250000	0,30 %
I1-L-ORO.vsi - 20x	Rectangle	1444,7749	250000	0,58 %
Average		958,96	250000	**0,38 %**
J1-L-ORO.vsi - 20x	Rectangle	6300,8662	250000	2,52 %
J1-L-ORO.vsi - 20x	Rectangle	3521,5142	250000	1,41 %
J1-L-ORO.vsi - 20x	Rectangle	11034,6729	250000	4,41 %
Average		6952,35	250000	**2,78 %**
J2-L-ORO.vsi - 20x	Rectangle	2752,3601	250000	1,10 %
J2-L-ORO.vsi - 20x	Rectangle	1035,9052	250000	0,41 %
J2-L-ORO.vsi - 20x	Rectangle	3566,8137	250000	1,43 %
Average		2451,69	250000	**0,98 %**
K1-L-ORO.vsi - 20x	Rectangle	2265,9177	250000	0,91 %
K1-L-ORO.vsi - 20x	Rectangle	856,3499	250000	0,34 %
K1-L-ORO.vsi - 20x	Rectangle	1028,7465	250000	0,41 %
Average		1383,67	250000	**0,55 %**
K1-L-ORO.vsi - 20x	Rectangle	2265,9177	250000	0,91 %
K1-L-ORO.vsi - 20x	Rectangle	856,3499	250000	0,34 %
K1-L-ORO.vsi - 20x	Rectangle	1028,7465	250000	0,41 %
Average		1383,67	250000	**0,55 %**
K2-L-ORO.vsi - 20x	Rectangle	107,4985	250000	0,04 %
K2-L-ORO.vsi - 20x	Rectangle	617,4122	250000	0,25 %
K2-L-ORO.vsi - 20x	Rectangle	377,1835	250000	0,15 %
Average		367,36	250000	**0,15 %**
L2-L-ORO.vsi - 20x	Rectangle	22703,1875	250000	9,08 %
L2-L-ORO.vsi - 20x	Rectangle	18222,5195	250000	7,29 %
L2-L-ORO.vsi - 20x	Rectangle	39658,6094	250000	15,86 %
Average		26861,44	250000	**10,74 %**

Appendix C. Statistical Tests

Table C1: Shapiro-Wilk test. The null hypothesis of the Shapiro-Wilk test is that the data is normally distributed, and a p-value larger than 0.05 is interpreted as a failure to reject the null hypothesis (i.e., a p-value>0.05 means normal distribution). *BW = body weight, LW = liver weight, FM = fat mass, TG = triglycerides, ORO = Oil Red O, PSR = Picro Sirius Red, SBP = systolic blood pressure*

```
> Normality_BW     <- Normality_Function(Characteristics, "BW") #Normal

Shapiro-Wilk Test Results for BW :
Test Statistic = 0.960466265515853
p-value = 0.447863601486808
> Normality_LW     <- Normality_Function(Characteristics, "LW") #Normal

Shapiro-Wilk Test Results for LW :
Test Statistic = 0.919202584157091
p-value = 0.0560871265731417
> Normality_FM     <- Normality_Function(Characteristics, "FM") #Not normal

Shapiro-Wilk Test Results for FM :
Test Statistic = 0.891349977034959
p-value = 0.0141749039984306
> Normality_TG     <- Normality_Function(Characteristics, "TG") #Normal

Shapiro-Wilk Test Results for TG :
Test Statistic = 0.929367427819163
p-value = 0.105977530931232
> Normality_ORO     <- Normality_Function(Characteristics, "ORO") #Not normal

Shapiro-Wilk Test Results for ORO :
Test Statistic = 0.606377764154818
p-value = 1.55633840066227e-06
> Normality_PSR     <- Normality_Function(Characteristics, "PSR") #Not normal

Shapiro-Wilk Test Results for PSR :
Test Statistic = 0.881448604245594
p-value = 0.0227559383366041
> Normality_SBP     <- Normality_Function(Characteristics, "SBP") #Normal

Shapiro-Wilk Test Results for SBP :
Test Statistic = 0.946551854547814
p-value = 0.227855749956441
```

Table C2: Levene's Test for Homogeneity of Variance. The null hypothesis of the Levene's test is that the variance of the data points is similar across the intervention and control group (homoscedasticity). Each of these variables had a p>0.05 meaning that we fail to reject the null hypothesis. *BW = body weight, LW = liver weight, FM = fat mass, TG = triglycerides, SBP = systolic blood pressure.*

```
> print(levene_resultBW)
Levene's Test for Homogeneity of Variance (center = median)
      Df F value Pr(>F)
group  1  0.8007 0.3806
      22
> print(levene_resultLW)
Levene's Test for Homogeneity of Variance (center = median)
      Df F value Pr(>F)
group  1  1.7814 0.1956
      22
> print(levene_resultTG)
Levene's Test for Homogeneity of Variance (center = median)
      Df F value Pr(>F)
group  1  1.6258 0.2162
      21
> print(levene_resultSBP)
Levene's Test for Homogeneity of Variance (center = median)
      Df F value Pr(>F)
group  1  1.0877 0.3083
      22
```

Table C3: Independent samples t-test. Parametric test of body weight (BW), liver weight (LW), liver triglyceride content (TG), and systolic blood pressure (SBP).

Test	Mean of Fructose	Mean of Control	Statistic	P_Value	Significant	Confidence_Interval
BW	765.654167	674.704167	6.825790	1.027639e-06	Yes	[63.22, 118.68]
LW	26.245000	18.770000	11.222429	4.507978e-10	Yes	[6.09, 8.86]
TG	28.178333	11.532500	3.396662	3.541838e-03	Yes	[6.28, 27.01]
FM	1.795833	1.159091	2.802880	1.178406e-02	Yes	[0.16, 1.11]
SBP	134.916667	119.666667	2.775306	1.155541e-02	Yes	[3.8, 26.7]

Table C4: Wilcoxon Rank Sum Test. Non-parametric test of fat mass (FM), liver weight (LW), Oil Red O (ORO) staining, and Picro Sirius Red (PSR) staining.

	Variable	p_value	Significance	Test_Statistic
	<chr>	<dbl>	<chr>	<dbl>
1	FM	0.0102	Significant	117
2	LW	0.000000740	Significant	144
3	ORO	0.000494	Significant	114
4	PSR	0.545	Not significant	36

Appendix D. qPCR Analysis

Table D1: Results from Ref Finder. Ref Finder is a website used by the laboratory engineer to compare and evaluate the stability and reliability of reference genes. The geometric mean of HMBS and Cyclo were used.

	Ranking Order (Better--Good--Average)				
Method	1	2	3	4	5
Delta CT	HMBS	Cyclo	GAPDH	HPRT1	SDHA
BestKeeper	Cyclo	HMBS	GAPDH	SDHA	HPRT1
Normfinder	HMBS	Cyclo	GAPDH	HPRT1	SDHA
Genorm	Cyclo | HMBS		GAPDH	HPRT1	SDHA
Recommended comprehensive ranking	**HMBS**	**Cyclo**	**GAPDH**	**HPRT1**	**SDHA**

Table D4: Input data from qPCR to Excel qPCR analysis file.

Sample Name	Gene Name	Cq Mean	Cq Error	Sample Name	Gene Name	Cq Mean	Cq Error	GeoMean
F_L2L	CYCLO	20,42	1,55	F_L2L	HMBS	24,77	0,18	22,49
F_L1L	CYCLO	18,95	0,17	F_L1L	HMBS	24,51	0	21,55
F_J2L	CYCLO	19,43	0,01	F_J2L	HMBS	24,33	0,27	21,74
F_J1L	CYCLO	19,16	0,04	F_J1L	HMBS	23,66	0,42	21,29
F_I2L	CYCLO	18,72	0	F_I2L	HMBS	23,19	1,07	20,84
F_I1L	CYCLO	19,27	0,04	F_I1L	HMBS	23,48	0,96	21,27
F_F2L	CYCLO	18,76	0,09	F_F2L	HMBS	23,79	0,1	21,13
F_F1L	CYCLO	19,18	0,06	F_F1L	HMBS	24,36	0,04	21,62
F_C2L	CYCLO	22,14	0,01	F_C2L	HMBS	26,92	0,01	24,41
F_C1L	CYCLO	19,09	0,08	F_C1L	HMBS	24,93	0,66	21,82
F_A2L	CYCLO	19,55	0,05	F_A2L	HMBS	24,25	0,01	21,77
F_A1L	CYCLO	19,23	0,08	F_A1L	HMBS	24,03	0,45	21,50
C_K2L	CYCLO	19,1	0,46	C_K2L	HMBS	23,95	0,03	21,39
C_K1L	CYCLO	19,98	0,03	C_K1L	HMBS	25,7	0,06	22,66
C_H2L	CYCLO	19,06	0,08	C_H2L	HMBS	24,44	0,3	21,58
C_G2L	CYCLO	20,1	0,16	C_G2L	HMBS	25,2	0,4	22,51
C_G1L	CYCLO	19,56	0,01	C_G1L	HMBS	24,73	0,02	21,99
C_E2L	CYCLO	20,27	0,16	C_E2L	HMBS	25,5	0,15	22,74
C_D2L	CYCLO	18,75	0,23	C_D2L	HMBS	23,74	0,16	21,10
C_D1L	CYCLO	18,32	0,08	C_D1L	HMBS	23,7	0,07	20,84
C_B2L	CYCLO	19,55	0,05	C_B2L	HMBS	24,6	0,22	21,93
C_B1L	CYCLO	19,28	0,04	C_B1L	HMBS	24,33	0,25	21,66
Efficiency		**0,98**				**0,93**		**0,95**

Table D4: Input from qPCR.

	Efficiency	Efficiency	Efficiency	Efficiency	Efficiency	Efficiency	Efficiency	Efficiency	Efficiency
	0,95	1,15	0,97	1,07	1,03	1,02	1,06	1,06	1,00
Control	**Geomean**	**COL1a1**	**PDK4**	**PPARa**	**FGF21**	**PPARy**	**ATF4**	**CHOP**	**PGC1a**
C_K2L	21,39	27,80	22,36	26,30	25,28	27,05	24,08	25,63	26,34
C_K1L	22,66	29,23	21,82	27,78	27,67	26,93	25,02	26,23	28,02
C_H2L	21,58	26,11	22,19	28,76	25,39	26,71	24,06	25,59	28,35
C_G2L	22,51	28,45	23,17	27,75	29,57	28,12	25,28	26,35	27,52
C_G1L	21,99	28,62	23,11	29,14	27,75	27,10	24,57	26,48	29,10
C_E2L	22,74	27,00	23,92	30,58	27,02	27,98	25,63	29,19	29,01
C_D2L	21,10	26,63	22,34	29,72	26,35	27,22	23,68	25,01	26,79
C_D1L	20,84	25,39	22,46	31,64	25,83	25,67	22,79	25,29	26,16
C_B2L	21,93	28,58	23,27	30,39	25,02	27,75	24,81	29,98	29,46
C_B1L	21,66	27,93	22,83	28,96	27,66	26,91	23,91	26,38	27,95
Fructose		**COL1a1**	**PDK4**	**PPARa**	**FGF21**	**PPARy**	**ATF4**	**CHOP**	**PGC1a**
F_L2L	22,49	27,73	21,44	27,44	24,49	27,72	23,99	26,06	27,36
F_L1L	21,55	27,48	22,44	27,29	24,45	27,31	23,87	25,54	27,39
F_J2L	21,74	27,76	22,40	27,54	24,07	27,19	24,23	25,80	27,79
F_J1L	21,29	26,16	21,94	28,49	21,94	26,89	22,40	25,31	28,73
F_I2L	20,84	27,14	22,04	27,01	20,14	26,98	22,21	24,74	26,83
F_I1L	21,27	27,90	22,61	27,82	21,26	27,58	23,32	25,61	27,53
F_F2L	21,13	27,38	21,79	27,88	23,23	25,90	22,77	24,68	27,70
F_F1L	21,62	25,96	22,35	28,61	24,14	26,79	24,04	26,11	28,49
F_C2L	24,41	28,53	24,39	35,30	27,35	28,81	26,77	28,48	29,00
F_C1L	21,82	28,50	20,97	29,53	22,02	26,10	23,24	25,92	26,92
F_A2L	21,77	28,56	22,13	31,14	26,59	26,17	24,84	26,42	27,76
F_A1L	21,50	28,38	22,79	29,42	25,84	26,90	23,77	25,83	26,87

Table D5: Results from qPCR analysis.

	Control	Fructose	Gene
Mean	0,00190581661421287	0,00172713607055350	*Col1a1*
SEM	0,00046658039059277	0,00038130961718503	
p=0.767			
Mean	3,67693121067301000	0,66238360841263900	*Pdk4*
SEM	1,51307623683515000	0,12214487558568300	
p=0.041			
Mean	0,00261958927551395	0,00237639392898464	*Ppara*
SEM	0,00089432798169353	0,00058085552594327	
p=0.816			
Mean	0,01712825406697680	0,18700169485318500	*Fgf21*
SEM	0,00423779557361139	0,06172032408990740	
p=0.021			
Mean	0,01182541043019580	0,01277057474548980	*Ppary*
SEM	0,00147316621917480	0,00166479894916154	
p=0.681			
Mean	0,04923657837733320	0,07758119502368740	*Atf4*
SEM	0,00394465330271524	0,00960169092413511	
p=0.019			
Mean	0,01279253307758900	0,01617976129756980	*Ddit3*
SEM	0,00214819012088227	0,00115709106893160	
p=0.161			
Mean	0,01033243867911890	0,01097974260076720	*Ppargc1a*
SEM	0,00179109003536807	0,00170783751433929	
p=0.797